

Section 7

**Global and regional climate models,
sensitivity and impact experiments,
response to external forcing**

Geographical Distribution of Internal Variability in Regional Climate Downscaling

ADELINA ALEXANDRU, RAMON DE ELIA* AND RENÉ LAPRISE

Département des sciences de la Terre et de l'Atmosphère, UQÀM & Ouranos Consortium*

e-mail : adelina@sca.uqam.ca

1. Introduction

Regional Climate Models (RCMs), are commonly used to overcome Global Climate Models (GCMs) poor resolution by adding fine-scale details upon the GCMs large-scale flow. Due to nonlinearities in the model physics and dynamics, RCMs can produce different time evolutions of simulated fields if a small perturbation affects the initial conditions (IC). This sensitivity, usually called internal variability, is partially controlled by the lateral boundary forcing, and hence size and geographical location of the integration domain play an important role. Internal variability of RCMs is in general smaller than that of GCMs. It is important to evaluate the internal variability of the RCMs, because it can mask physically forced signals and hence disturb the assessment of climate sensitivity to forcings.

2. Methodology

The model used in the present study is the Canadian RCM (CRCM). The CRCM is a limited-area model based on the fully compressible Euler equations solved by a semi-implicit and semi-Lagrangian numerical scheme. The model uses the physical parameterization package of the second generation CGCM with Bechtold-Kain-Fritsch deep and shallow convective parameterization. The computational points are fixed on a three-dimensional staggered grid projected onto polar-stereographic coordinates in the horizontal and Gal-Chen terrain-following levels in the vertical (for a detailed description of the model, see Caya and Laprise 1999).

The domain contains 121×121 grid points located over eastern North America and part of the Atlantic ocean at 45-km resolution. In the vertical, 18 Gal-Chen levels are distributed from the ground to the model's lid at 30 km. The integration time step is 15 minutes and the model is driven by 6 hours NCEP reanalyses.

An ensemble of 20 simulations began between May 1st and 20th, 1993 at 00 UTC and ending on September 1st, 1993 at 00 UTC is used in this study. All the runs overlap in June, July and August of 1993 and have a spin up period varying from 11 to 30 days. The integrations share exactly the same lateral boundary conditions (LBC) and have a delay of 24 hours between the beginning of one run and the beginning of the next.

The internal variability was estimated by computing the ensemble inter-member standard deviation (spread) as:

$$\sigma_{en}(x, y, t) = \sqrt{\frac{1}{M} \sum_{m=1}^M (X_m(x, y, t) - \langle X \rangle(x, y, t))^2} \quad (1)$$

where M is the number of ensemble members and $X_m(x, y, t)$ refers to the value of the variable X on grid point (x, y) at time t for the member m of the ensemble. The term $\langle X \rangle(x, y, t)$ is the ensemble mean defined as

$$\langle X \rangle(x, y, t) = \frac{1}{M} \sum_{m=1}^M X_m(x, y, t). \quad (2)$$

In addition, the time average of σ_{en}^2 gives an estimation of average spread for the entire season and its geographical distribution:

$$\sigma(x, y) = \sqrt{\frac{1}{NT} \sum_{t=1}^{NT} \sigma_{en}^2(x, y, t)}, \quad (3)$$

where NT refers to time step number.

3. Results and analyses

Figure 1 shows the time evolution of inter-member standard deviation (averaged on the entire domain) for the precipitation and geopotential fields. It is interesting to note the pulsating behavior of internal variability for both

precipitation and geopotential and that the most important maxima for the both fields are recorded at the middle and ending of the season. An analysis of the synoptic situation at the time of these maxima shows that heavy precipitation in the south of the US induced not only an important divergence between the precipitation ensemble members, but also a divergence among the geopotential ensemble simulations which continues to develop following the general circulation and reaches its maximum toward the northeast of the domain. This perturbation pattern is repeated several times during the three months (mostly concentrated in July) and leaves its trace in the seasonal average (Fig.2). Average precipitation spread maximum (14 mm/day is located in the south of the US where it was recorded a large quantity of precipitation (Fig.2a), while the average geopotential spread maximum is located at the northeast of the domain (Fig.2b).

4. Discussion

The results show that the CRCM's internal variability, estimated as standard deviation between 20 ensemble simulations differing slightly only in the IC, depends strongly on synoptic events. The dependence is clearly observed in the pulsating behavior of the time evolution of the inter-member spread. These variations have a preferential region, depending on the variable. We showed that in convective areas (e.g., south of the US), large quantities of precipitation induce important differences between the simulations. Also, we noticed that the geopotential spread is maximized to the northeast of the domain, region abundant in extra-tropical cyclones. Evaluation of time evolution of synoptic patterns suggests that the maximum in precipitation and geopotential are linked: the former being the trigger of a perturbation that develops in cyclonic circulations and attains the maximal spread before leaving the domain (not shown).

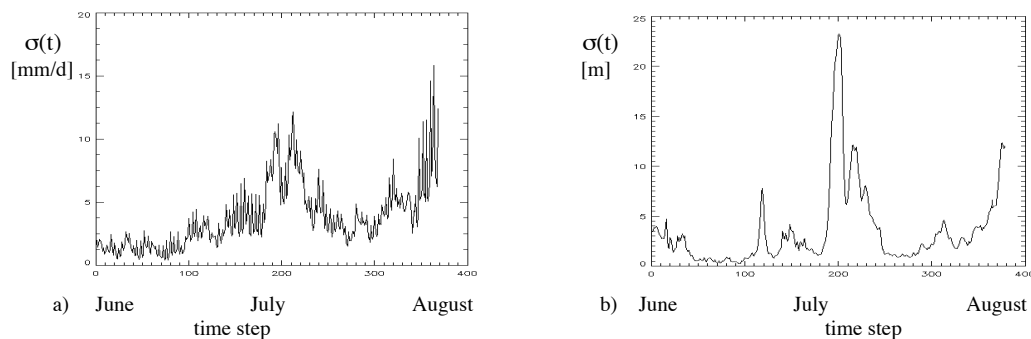


Figure1 : Time evolution of inter-member standard deviation for the precipitation a) and for the 850-hPa geopotential b).

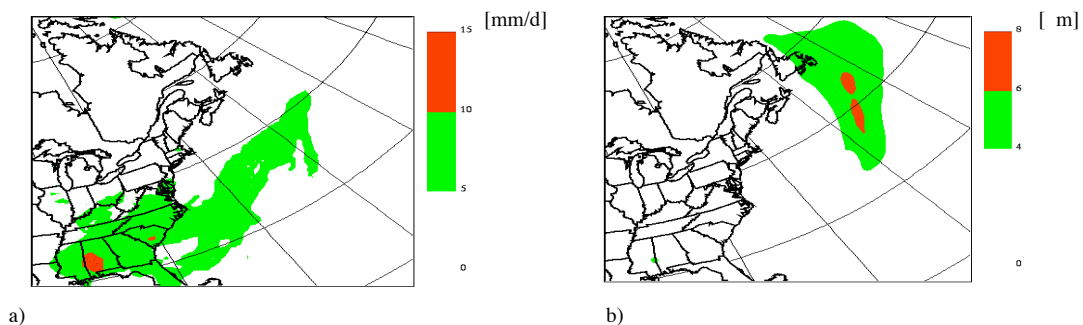


Figure 2 : Square root of 3-month time average of inter-member variance for the precipitation a) and for the 850-hPa geopotential b).

References :

Caya, D. and R. Laprise, 1999; Mon. Wea. Rev., 127, 341-362.

Modelling thermal and hydrologic regime of the permafrost

M.M. Arzhanov, P.F. Demchenko, A.V. Eliseev, I.I. Mokhov

A.M. Obukhov Institute of Atmospheric Physics RAS,
3 Pyzhevsky, 119017, Moscow, Russia, e-mail: arzhanov@ifaran.ru

The model for thermal and hydrological regime of the soils, which is suitable for the climate model of intermediate complexity, is developed. The soil model numerics is based on the method of "phase boundary catching" [1]. The soil hydrology is computed, based on [2], but with the runoff, parameterized in accordance to [3].

Here, this model is applied to the computation of the active layer thickness (ALT) in the Northern Hemisphere. The model has been forced by the monthly NCEP/NCAR reanalysis climatology for 1979-1995. For simplicity, the soil heterogeneity is neglected and everywhere the soil thermo/hydrophysical parameters, corresponding to loam, are prescribed. The computed ALT is shown in Fig. 1.

The total area, covered by permafrost in the model, is about 21 mln.sq.km. This is quite close to the observationally based estimate ~23 mln.sq.km [4]. This value is also agree with the continuous potential permafrost area 20 mln sq.km, estimated, using the severity index [5] (with the surface air temperature, again taken from the NCEP/NCAR reanalysis dataset). Moreover, the geographical boundaries of the regions, where the permafrost is simulated by the model, are in the good agreement with the severity index isoline, bounding the continuous potential permafrost.

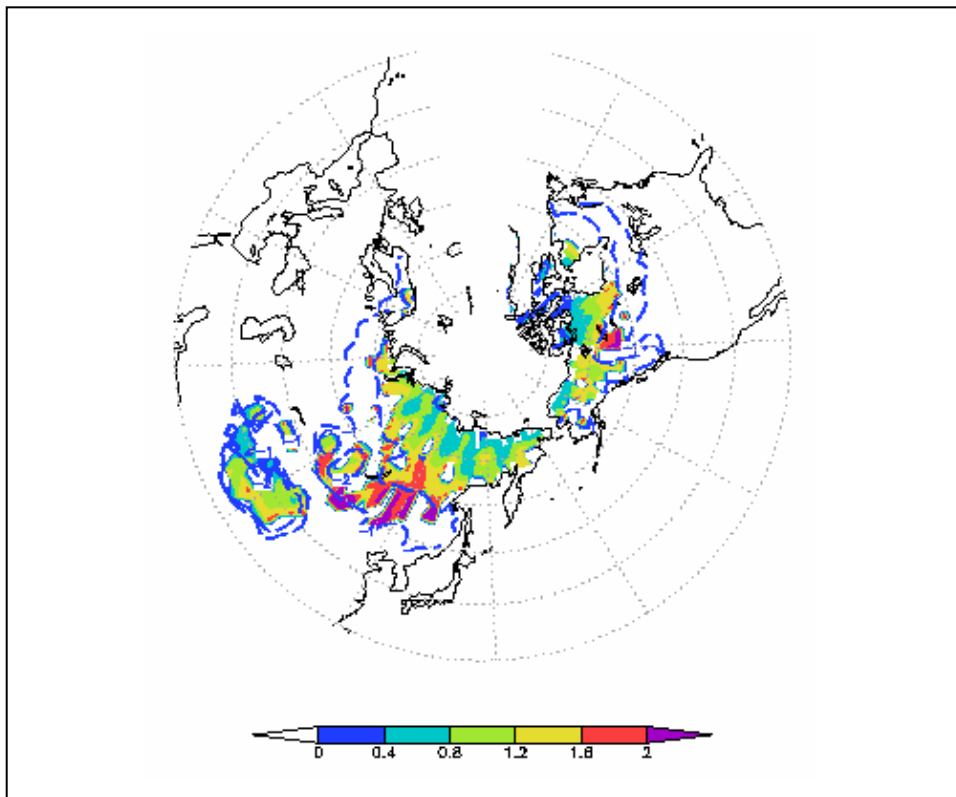


Fig.1: Simulated active layer thickness (color shades) together with the severity index isolines -1 and -2 (bounding sporadic and continuous potential permafrost, respectively).

The computed ALT can be compared with the results of the direct measurements, performed in the limited number of experimental sites. Here, this comparison is performed for the site near Yakutsk (62N 129E). The modeled value is 1.3 m, while the measurements embed the range 1.4-1.7 m with the mean value 1.5 m [6]. This underestimation can be due to cold bias in the NCEP/NCAR reanalysis (note that the area, covered by the continuous potential permafrost in this reanalysis, is close to the observationally estimated area, covered by the all types of permafrost).

References:

1. Anisimov, O.A., 1989: On estimation of the permafrost sensitivity to the global thermal regime of the Earth's surface. *Sov. Meteorol. Hydrol.*, (5), 79-84.
2. Pachepsy, Ya.A., L.B. Pachepskaya, E.V. Mironenko, and A.S. Komarov, 1976: Modelling the water-salt regime of soils using computer. Nauka Publ. House, Moscow [in Russian].
3. Volodin, E. M. and V. N. Lykosov, 1998: Parametrization of Heat and Moisture Transfer in the Soil–Vegetation System for Use in Atmospheric General Circulation Models: 1. Formulation and Simulations Based on Local Observational Data. *Izvestia, Atmos. Oceanic Phys.*, 34 (4), 405-416.
4. Zhang, T., R.G. Barry, K. Knowles, J.A. Heginbottom, and J. Brown, 1999: Statistics and characteristics of permafrost and ground-ice distribution in the Northern Hemisphere. *Polar Geogr.*, 23(2), 132-154
5. Demchenko, P.F., A.A. Velichko, A.V. Eliseev, I.I. Mokhov, and V.P.Nechaev, 2002: Dependence of permafrost conditions on global warming: Comparison of models, scenarios, and paleoclimatic reconstructions. *Izvestia, Atmos. Oceanic Phys.*, 38 (2), 143-151
6. Pavlov, A.V., 2003: Permafrost and climate changes on the north of Russia: Observation and forecast. *Izvestiya, Geogr.*, (6), 39-50 [in Russian]

Association between sea surface temperature over the North Atlantic Ocean and the summertime convection over the South America

Rosane Rodrigues Chaves

Universidade Estadual do Norte Fluminense Darcy Ribeiro - UENF

Laboratório de Meteorologia - LAMET

Macaé - Rio de Janeiro - Brazil

rosane@lenep.uenf.br

1. Introduction

In contrast to the sea surface temperature (SST) over the South Atlantic Ocean (Robertson e Mechoso 2000, Chaves e Nobre 2004 and Chaves e Ambrizzi 2005), the influence of the SST over the North Atlantic Ocean in the summer convection over the South America (AS) does not have received attention from the research community. In this study was evaluated the association between the SST over the North Atlantic Ocean (Equador-40°N; hereafter referred as NA) and the summer convection over the SA through statistical methods as Principal Components Analysis (PCA) and numerical experiments with the CPTEC/COLA atmospheric general circulation model. The observational analysis used SST from COADS and Outgoing Longwave Radiation (OLR) from CDC/NOAA. Patterns of SST anomalies over the NA were determined through PCA to December-January-February (DJF) from 1979 to 2001. Association of these patterns with summertime convection over the SA was determined by linear correlation between the time series of these patterns and OLR anomalies over this continent. The CPTEC/COLA model was used to perform sensitivity experiments with prescribed boundary conditions over the NA in order to evaluate the association between SST over this ocean region and the summertime convection over the SA. Three numerical experiments were done from November 2000 to February 2001. A control run was carried out by using observed global SST from NCEP as surface ocean boundary condition. This experiment was referred as *CTR*. The others two experiments used a negative and a positive increment added over the NA, and observed global SST over the remaining oceans. These experiments were referred as *AFN* and *AQN*, respectively. The AGCM was integrated for 120 days, with 5 distinct initial conditions from NCEP operational analysis for 12:00 UTC on 1 November 1995, 1996, 1998, 1999 and 2000 for all experiments (*CTR*, *AFN* and *AQN*). The December 2000 to February 2001 ensemble averages for each experiment were analyzed.

2. Results

The spatial pattern associated with the first anomalies SST mode shows one monopole pattern over the NA (not showed). The second pattern shows an out-of-phase relationship between SST anomalies over the tropical and subtropical regions (not showed). The third pattern shows three action centers over the NA, SST anomalies with same signal over equatorial and subtropical regions and different signal over intermediate region (Fig. 1a). The first and third patterns show greater interannual variability and the second pattern interdecadal variability. Only the third mode has influence over summertime convection on the SA. It explains 9.4% of the variance. This third pattern shows correlation significant with summertime convection only over the northernmost part of this continent (Fig. 1b). The convection in this region is associated with positive SST anomalies over equatorial and subtropical region and negative SST over the tropical part of the NA. Results from numerical experiments corroborate the

results of the observational analysis; indicate also that SST over the NA has influence only in the summertime convection over the northernmost part of the SA (Fig. 2a, b).

3. Conclusions

The results of the observational analysis and numerical experiments showed that the SST over the NA (Equator e 40°N) has influence only in the summer convection over the northernmost part of the SA, with warm SST anomalies there associated with the convection over this continental region. Thus, apparently, the SST over the NA was not important for the predictability of the summer convection over most of the SA, included the South Atlantic Convergence Zone, to DJF from 1979 to 2001. Results presented here were based on statistical methods with dataset from DJF 1979 to 2001 and CPTEC/COLA model simulations with prescribed boundary conditions. In order to evaluate the dependence of these results, they must be compared with others models and observational data.

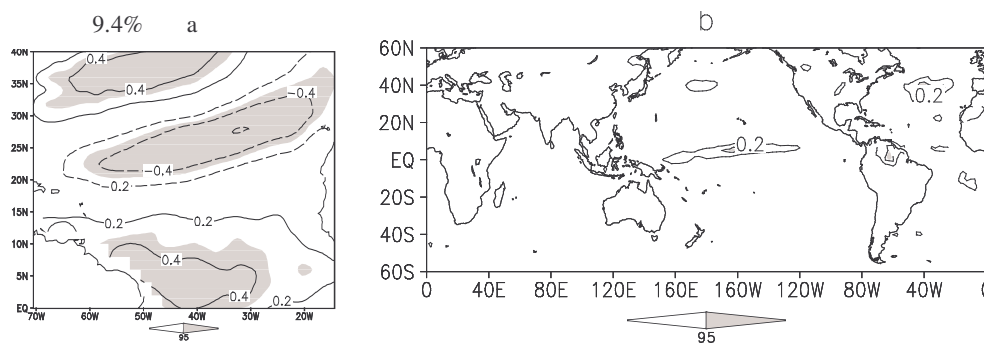


Figure 1 - Third EOF modes of the SST anomalies over the North Atlantic Ocean to DJF from 1979 to 2001 (a) and correlation field between time series of expansion coefficients of this EOF modes and OLR anomaly at that grid point between 60°S and 60°N from 1979 to 2001. The shaded areas represent statistical significance at the 95% confidence level.

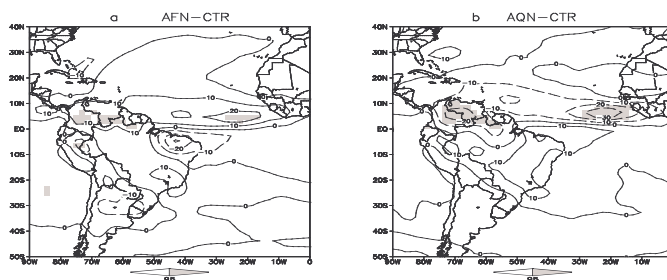


Figure 2 - OLR difference between AFN and CTR (a), AQN and CTR (b) experiments. The shaded areas represent statistical significance at the 95% confidence level.

4. References

- Chaves, R. R.; Nobre, P. Interactions between sea surface temperature over the South Atlantic Ocean and the South Atlantic Convergence Zone. *Geophys. Res. Lett.* 31:L03204, 2004.
- Chaves, R R.; Ambrizzi, T. Atmospheric response for two convections schemes in sensitivity experiments using SST anomalies over the South Atlantic Ocean. *CLIVAR Newsletter Exchanges Seasonal Predictability*, **33**, 2005.
- Robertson, A. W.; Mechoso, C. R. Interannual and Interdecadal Variability of the South Atlantic Convergence Zone. *Mon. Wea. Rev.*, **128**:2947-2957, 2005.

Effects of resolution in an RCM: From 50 to 12 km

O. B. Christensen, J. H. Christensen and A. Guldberg

Danish Meteorological Institute, Lyngbyvej 100, 2100 Copenhagen, Denmark

e-mail: obc@dmi.dk, jhc@dmi.dk and ag@dmi.dk

Simulations in 3 different resolutions with the Danish regional climate model HIRHAM has been performed and results showing the effect of resolution on the distribution of precipitation are presented.

The HIRHAM model has been run in a rotated latitude-longitude system with 0.44, 0.22, and 0.11 degrees resolution, roughly corresponding to 50km, 25km, and 12km grid distance, for a domain covering all of Europe. The experiments were run for 2x30 years, a control period (1961-1990) and a scenario period (2071-2100) in accordance to the SRES emission scenario A2.

The boundary conditions consisted of atmospheric fields and sea-surface temperatures from time slice simulations with the high-resolution atmospheric global model HadAM3H from the British Hadley Centre in 1.875x1.25 degrees resolution from the PRUDENCE project (boundary values available at 3.75x2.5 degrees). These time slices receive SSTs from either observations (1961-1990) or in the scenario experiment observations plus an anomaly calculated with the coupled global model HadCM3.

Average precipitation in general, and the effects of orography in particular for a transect through the Alps are compared to the observational data set collected at the ETH in figure 1 and 2.

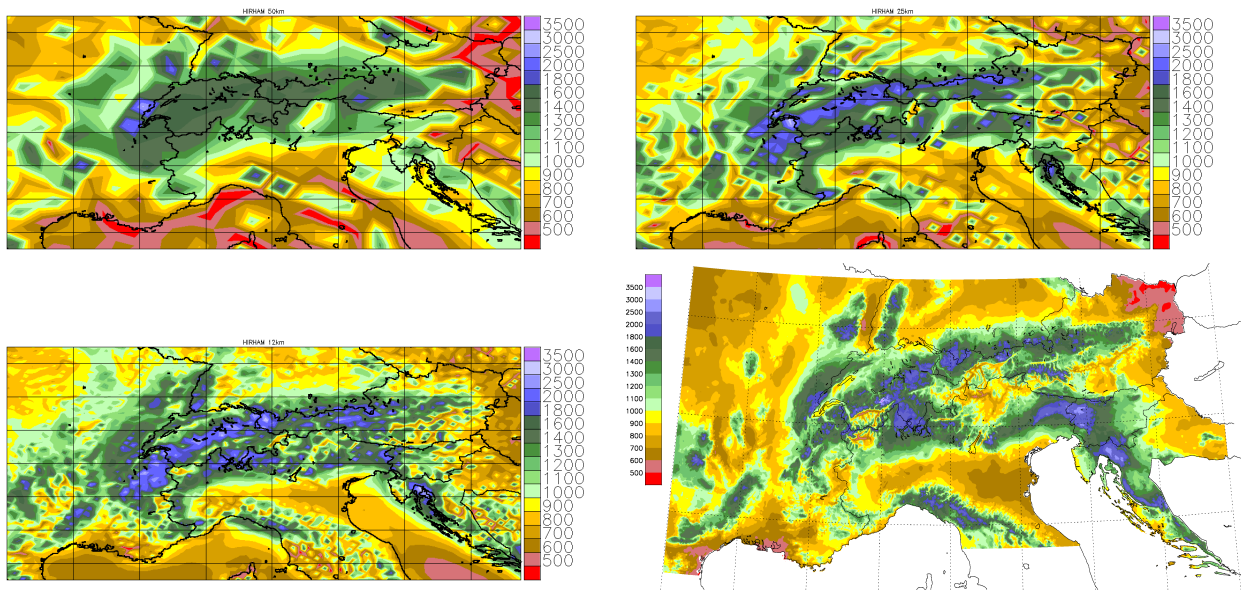


Figure 1. Long-time average of precipitation in the Alps as simulated by HIRHAM in 50 km (upper left figure), 25 km (upper right) and 12 km (lower left) resolution compared to observed climatology (lower right). (Unit: mm/year)

A higher resolution in regional climate simulations is seen to dramatically improve the distribution of precipitation in complex terrain. The very narrow boundary relaxation zone used in these simulations and the absence of a retuning of the physical parameterization does not decrease the quality of large-scale climate features.

Precipitation connected with land-sea contrast has a tendency to fall over water in lower resolution, but moves realistically further inland in higher resolution; see the coast of Croatia in the maps of average precipitation.

In the Alpine transect shown in figure 2, the experiments in 25 and 12 km resolution both show a realistic pattern with maxima in precipitation on the slopes and local minima on the mountain tops; in contrast to this, the 50km experiment shows one broad precipitation maximum, coinciding

with mountain tops. For the length scales of this particular mountain chain the important change in realism occurs between 50 and 25 km resolution. For other, smaller orographic features like the Rhône valley or the Apennines there seems to be a transition between 25 and 12 km.

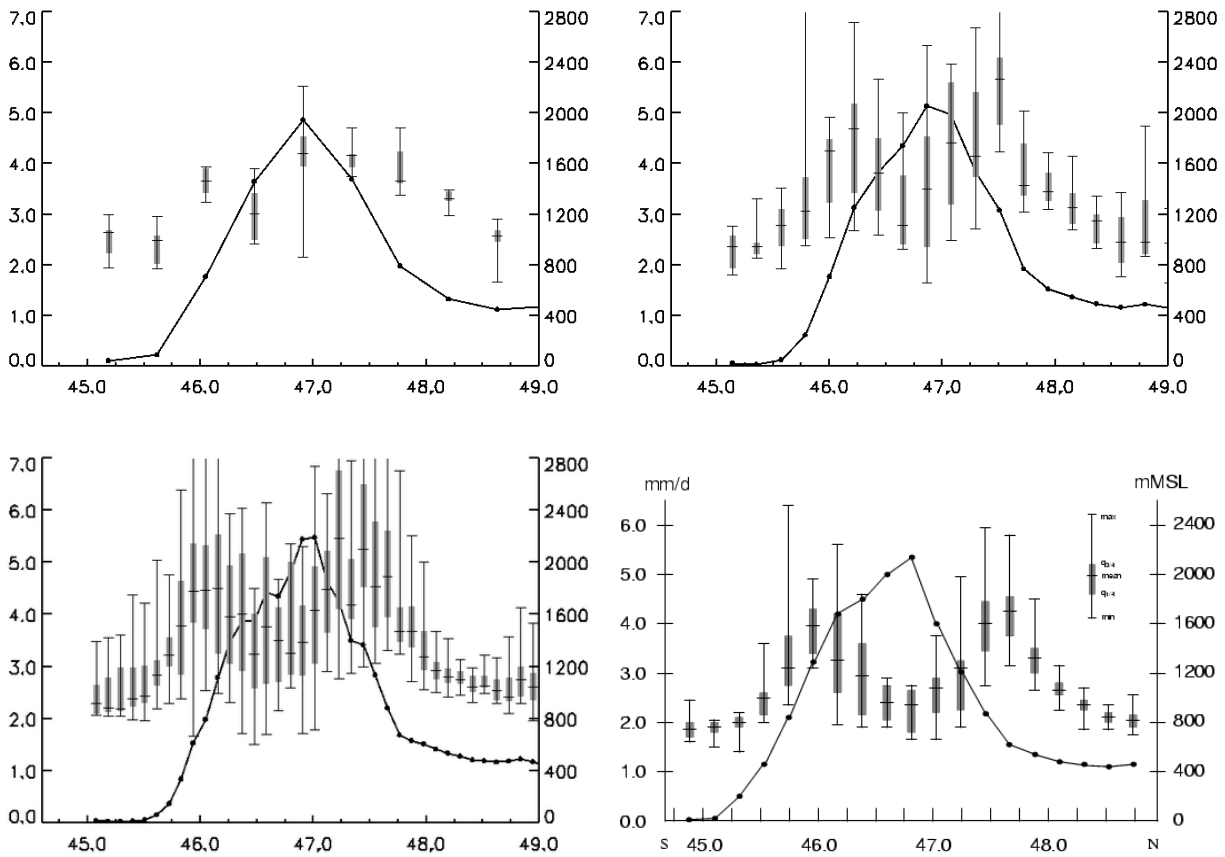


Figure 2. Annual precipitation as a function of latitude for transects through the Alps between 45 and 49 degrees north and 11 and 13.5 degrees east simulated by HIRHAM in 50 km (upper left figure), 25 km (upper right) and 12 km (lower left) resolution. Thick error bars mark quartiles and thin bars mark extremes across each (model) latitude. The lower figure from Frei and Schär (Int. J. Climatol., 18, 873-900, 1998) shows station data and quantiles from these and are hence not directly comparable to the model results. (Unit: left axis: mm/day, right axis: m above sea level)

Preliminary analysis of the simulations indicate that climate change signals do not show a lot of resolution influence when relative changes are studied. However, this means that absolute precipitation changes are quite different between the different resolutions. This has the consequence that investigations of climate effects on the hydrological cycle in mountain areas like the Alps and in coastal areas are greatly improved by a higher resolution. Examining the intense winter precipitation we again see very little resolution influence on the relative change. Again, this of course means that absolute values will be much more realistically described in a high-resolution experiment. Comparing the relative change in average and the more intense precipitation for the 50km experiment it is seen that the intensity distribution generally just scales, i.e., the change in occurrence of intense precipitation follows what should be expected from the change in average precipitation; there is no general change in the number of wet days or in the shape of the intensity distribution. Further analysis of these experiments will be performed.

Hydrology of Northern Quebec as seen by the Canadian Regional Climate Model.

Anne Frigon¹, Michel Slivitzky¹ and Daniel Caya¹

¹Ouranos, Montréal (Québec), Canada, frigon.anne@ouranos.ca

Results from five simulations performed with the Canadian Regional Climate Model (CRCM; Caya and Laprise 1999) are used to compare simulated hydrologic regimes with observations over 21 basins over the Québec/Labrador peninsula. Basins of interest cover areas ranging from 13 000 to 177 000 km², for a total area of 1 000 000 km².

Four of these simulations were driven by NCEP/NCAR global atmospheric reanalyses (NRA1; Kalnay et al. 1996) and the other was driven by ERA40 (European Center for Medium-Range Weather Forecasts reanalyses; Gibson et al. 1997); both reanalyses used are freely available at a 2.5x2.5 degree resolution. One simulation, NRA1 driven, was performed over a large domain covering North America (AMNO; 201x193 grid points) while the four others were done over a smaller domain centered over Québec (QC; 112x88). One simulation over the QC domain used a simple one-layer surface scheme, while the four others were run with the CLASS multi-layer surface scheme (Canadian LAnd Surface Scheme; Verseghy 2000). Spectral nudging of large-scale winds (Riette and Caya 2002) keeps CRCM's large-scale flow close to its driving data and was applied to the run over the large AMNO domain and to two simulations performed over the smaller QC domain (driven by NRA1 and ERA40). All simulations were driven by 6-hourly reanalyses over the 1959–99 period (linearly interpolated to the model's 15-minute time steps) with a horizontal grid-size mesh of 45 km (true at 60°N) and 29 vertical levels, unequally spaced from the surface to the model top (29 km). Over ocean grid points, values of sea surface temperature and sea-ice cover from AMIP II monthly observations were used.

A subset of ten basins, covering a total area of 406 000 km² (Rivière à la Baleine, Bell, Réservoir Caniapiscou, Réservoir Churchill Falls, Georges, Réservoir Manic5, Caniapiscou-Pyrite, Rupert, Lac Saint-Jean, Waswanipi), were chosen to perform comparative analyses on the influence of (1) domain characteristics, (2) the surface scheme and (3) driving data, on surface hydrologic budget components. The choice of basins was motivated by the availability of reliable and long series of runoff observational data. Over this 10-basin composite, we compare climatologic means (over the 1961–90 period) simulated by the CRCM with annual runoff and precipitation observed during the same period. When required, observed annual runoffs were corrected for variability introduced by anthropogenic water storage. Monthly precipitation series from the Climatic Research Unit (CRU TS2.02; Mitchell and Jones 2005) and from University of Delaware (WM 1.02; Willmott and Matsuura 2001) were interpolated from their global grid to the CRCM's polar stereographic grid. Finally, composite results over the 10 or 21 basins were computed by weighing each basin value according to the number of grid points located within the basin.

We find that domain size has an influence on simulated annual precipitation and runoff. In the 1961–90 period, over the 10-basin composite, the large domain CRCM simulation generates 0.27 mm/day less precipitation and runoff than the small domain run, which represents –13% for precipitation and –19% for runoff (both runs with CLASS and NRA1 driven).

The choice of the surface scheme seems to have less influence than domain size on simulated annual runoff. However, it is not negligible, since the CRCM simulation with CLASS shows a difference of –0.08 mm/day (–6%) when compared to the simulation using the one-layer surface scheme (both runs on QC domain and NRA1 driven).

Different reanalyses used as driving data have an influence comparable to that of the surface scheme. With respect to the NRA1 driven CRCM simulation, the ERA40 driven run has values larger by about 5% over the 10-basin composite for the 1961–90 period, giving absolute differences of +0.13 mm/day for precipitation and +0.08 mm/day for runoff (both runs with CLASS on QC domain).

Over the 10 basins, the CLASS/QC/ERA40 simulation is found to be the best of the five CRCM runs. With respect to observations, it shows simulated annual biases of only –2% for precipitation and –10% for runoff, which is considered to be within the observational error associated to water related variables.

Fig. 1 shows that CRCM's mean annual runoffs differ for the 10-basin composite when the simulation is driven by NRA1 and by ERA40 (both runs with CLASS on QC domain). This is the case, even though standard deviations are quite comparable for both simulations in the 1961–99 period (0.17 mm/day for

NRA1 driven run and 0.18 mm/day for ERA40 driven run). Correlations with annual 1961–99 observations also remain comparable for both runs ($R=0.82$ vs 0.81). These differences become more important when we examine individual basin behavior.

Finally, Table 1 summarizes CRCM simulation results over the 21-basin composite in the 1961–99 period. We find that the best run in regards to simulated mean annual runoff (CLASS/QC/ERA40) gives a root mean square difference (RMSD) value of 13% with a mean bias of only -3% . Considering each of the 21 basins, RMSD values range from 8 to 18%, without any apparent relation with the size of the basins or with their regional location (north vs south and east vs west).

Globally, over each of the 21 basins studied, in the 1961–99 period, simulated annual runoffs show biases with observations that vary from -15% to $+10\%$, while coefficients of determination span from near zero over some basins, to values reaching almost 0.7. There does not seem to be any relation between these two variables and their distribution appears random over the territory.

In conclusion, we find that, when driven by atmospheric reanalyses, the CRCM is capable of reproducing annual runoff within 15% over the study basins in regards to mean climatology as well as interannual variability. Domain size plays an important role on the bias as well as on correlation of annual runoff simulated by the CRCM; the choice of the surface scheme seems to have a weak but not negligible influence on the simulated annual runoff; the choice of atmospheric reanalyses (driving data) has an effect similar to that of the surface scheme.

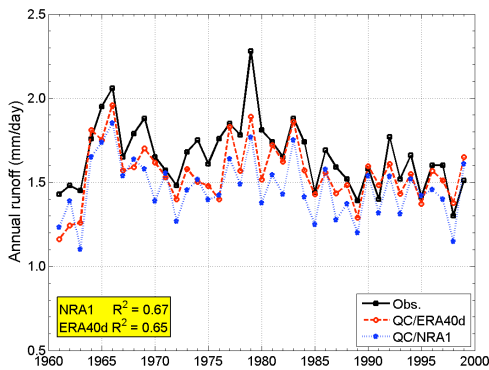


Fig. 1. Mean annual runoff over the 10-basin composite from two CRCM/CLASS simulations performed over the small QC domain, one being driven by NRA1 (dots) and the other by ERA40 (dash); continuous line shows observations.

	AMNO/ NRA1	QC/ NRA1	QC/ ERA40d
Obs. (mm/day)	1.57	1.57	1.57
CRCM (mm/day)	1.12	1.41	1.51
Bias (mm/day)	-0.46	-0.16	-0.06
Bias (%)	-29%	-10%	-3%
RMSD (mm/day)	0.51	0.26	0.21
RMSD (%)	32%	16%	13%

Table 1. Simulated 21-basin composite 1961–99 mean annual runoff from CRCM/CLASS, with different domains and driving data, compared with observations (Obs.).

References

Caya, D., and R. Laprise, 1999: A Semi-Implicit Semi-Lagrangian Regional Climate Model: The Canadian RCM. *Mon. Wea. Rev.*, **127**, 341-362.

Gibson, J.K., P. Killberg, S. Uppala, A. Hernandez, A. Nomura, and E. Serrano, 1997: ERA description, *ECMWF Reanalysis Project Report Series No. 1*, European Centre for Medium-Range Weather Forecasts, Reading.

Kalnay, E., M. Kanamitsu, R. Kistler, W. Collins, ... 1996: The NCEP/NCAR 40-Year Reanalysis Project. *Bull. Amer. Meteor. Soc.*, **77(3)**, 436-472.

Mitchell, T.D., and P.D. Jones, 2005: An improved method of constructing a database of monthly climate observations and associated high-resolution grids. *Int. J. Climatol.*, **25(6)**, 693-712.

Riette, S. and D. Caya, 2002: Sensitivity of short simulations to the various parameters in the new CRCM spectral nudging. *Research activities in Atmospheric and Oceanic Modelling*, edited by H. Ritchie, WMO/TD-No 1105, Report No. 32: 7.39-7.40.

Versoghy, D.L., 2000: The Canadian LAnd Surface Scheme (CLASS): Its history and future. *Atmos.-Ocean*, **38**, 1-13.

Willmott, C.J., and K. Matsuura, Monthly precipitation time series (1950-1999), version 1.02, released July 1, 2001; <http://climate.geog.ude.edu/~climate/>

Assessing linkages between climate variability in high-latitudes and the tropics with ENSO forcing in GCM simulations of polar climate proxies

Scott Gregory and David Noone

Department of Atmospheric and Oceanic Sciences, and Cooperative Institute for Research in Environmental Sciences, University of Colorado, Boulder, CO, USA
(email: Scott.Gregory@colorado.edu)

The coupling between climate variability and change at high latitudes and the tropics is not well understood. Teleconnection patterns have been used to explain covariation between Arctic sea ice and the monsoon (e.g., Chang *et al.*, 2003), while some studies suggest a tropical driver of high latitude conditions (e.g., Turney *et al.*, 2005). Nonetheless, it is clear that the implied linkages give rise to regionally organized patterns of climate variability that play an important role in climate reconstruction because local influences on proxies could otherwise be incorrectly interpreted as global change. To this end, it is unclear if the strength of the coupling, and the structure of teleconnection patterns, remains constant in the presence of natural and anthropogenic forcing. As a case in point, Schneider *et al.* (2005) have shown that climate change inferred from isotope proxies in Antarctica differs from that of the Southern Hemisphere and global instrumental records. Their analysis shows that a substantial part of this change is associated with changes in the mean amplitude of the Southern Annular Mode, but also implicates change associated with the El Niño-Southern Oscillation (ENSO). Both of these regional patterns are known to be an important aspect of Antarctic climate (Turner *et al.*, 2005).

The NCAR Community Atmosphere Model Version 3 (CAM3) is used to develop an understanding of the coupling between the tropics and high latitudes by simulating the stable water isotope composition of polar snow for different phases of ENSO and investigating the physical mechanisms that drive the associated isotopic changes. To do so, the circulation associated with ENSO must first be reproduced. Forcing ENSO conditions by prescribing SST anomalies produces an acceptable representation of geopotential height anomalies associated with El Niño when compared to NCEP reanalysis (Figure 1). Similar results are found with La Niña forcing. With an emphasis on accurate simulation of circulation and water transport in the Antarctic, an additional experiment is forced by introducing a bias directly into the surface pressure tendency equation. Specifically, the surface pressure anomalies associated with ENSO from the NCEP reanalysis are used to nudge the surface pressure toward the observed conditions over a relaxation time of one day. A long relaxation time corresponds to a weaker forcing, and a short time to strong forcing. This method has the advantage that when used with a slab ocean model the land sea contrasts and stationary planetary waves are not artificially amplified as they are when fixed SSTs are used. Figure 1 shows that while this method results in broad agreement with the observed anomalies, the initial results do not reproduce the details of the observed anomalies as well as the experiment in which the SSTs were prescribed. This is in part due to a spatially uniform relaxation time that is tuned for midlatitude conditions. This acts to overemphasize the tropical influences relative to the mid and high latitudes and introduces a strong wave-like structure near the Antarctic Peninsula. Further refinement of the technique will vary the relaxation time with latitude that mimics the latitude dependent adjustment timescales of geophysical flows, and thereby constrain the high latitude circulation more reliably.

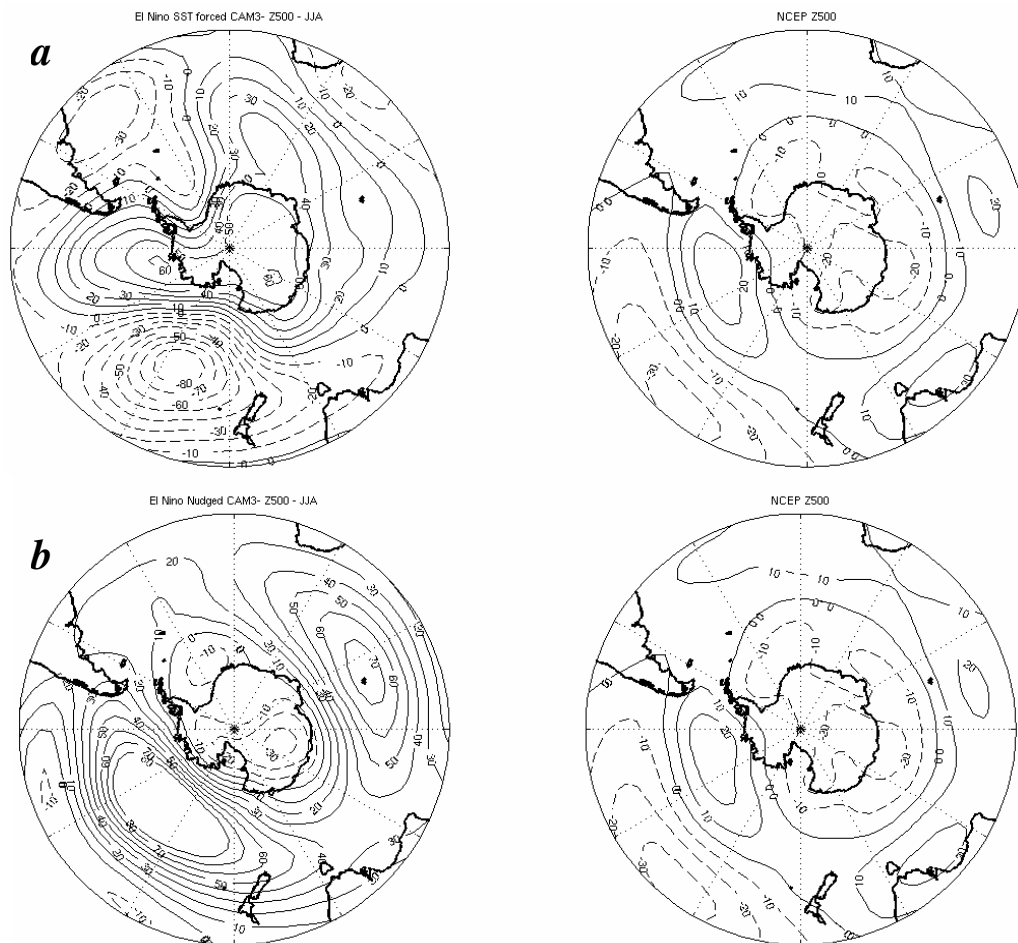


Figure 1: June-July-August average 500 hPa geopotential height anomalies associated with El Niño from 10-year CAM3 simulations forced with observed a) SST anomalies and b) surface pressure anomalies and the slab ocean model. Right panel shows equivalent anomalies from the NCEP Reanalysis as verification. The contour interval is 10 meters and negative contours are dashed.

Chiang, J. C. H., M. Biasutti, and D. S. Battisti, 2003: Sensitivity of the Atlantic Intertropical Convergence Zone to Last Glacial Maximum boundary conditions. *Paleoceanography*, **18**, 10.1029/2003PA000916.

Turner, J., S. R. Colwell, G. J. Marshall, T. A. Lachlan-Cope, A. M. Carelton, P. D. Jones, V. Lagun, P. A. Reid and S. Iagovkina, 2005: Antarctic climate change over the Antarctic during the last 50 years. *International Journal of Climatology*, **25**(2), 279-294.

Turney, C.S., A.P. Kershaw, S.C. Clemens, N. Branch, P.T. Moss, and L. K. Fifield, 2004: Millennial and orbital variations of El Niño/Southern Oscillation and high-latitude climate in the last glacial period, *Nature*, **428**, 306-310.

Schneider, D.P., E.J. Steig, and T. van Ommen: High-resolution ice core stable isotopic records from Antarctica: towards interannual climate reconstruction, *Annals of Glaciology*, **41**, in press.

Climate change over southern Africa

Stefan Hagemann and Daniela Jacob

Max Planck Institute for Meteorology, Bundesstr.53, 20146 Hamburg, Germany
Email: Hagemann@dkrz.de, Jacob@dkrz.de

Over the southern part of Africa, strong climatological gradients exist, ranging from the humid tropical climate in the Congo region to the drylands in the western part of South Africa, e.g. the Namib desert. Changes in the climatological gradient will alter the hydrological cycle over southern Africa, and thus may have significant consequences in the affected regions. Projected future changes are investigated using the recent version of the coupled atmosphere/ocean general circulation model of the Max Planck Institute for Meteorology. The model comprises the atmospheric component ECHAM5, the ocean component MPI-OM and the OASIS coupler. For the 4th assessment report of the Intergovernmental Panel on Climate Change (IPCC), an ensemble of climate simulations was conducted for the period of 1860-2100. The coupled model was run without flux correction at T63 (about 1.9° or 200 km grid size) horizontal resolution and 31 vertical levels in the atmosphere, and about 1.5° horizontal resolution and 40 vertical layers in the ocean. For the past climate (1860-2000), observed concentrations of CO₂, Methane, N₂O, CFCs, Ozone (tropospheric and stratospheric), and sulphate aerosols (direct and first indirect effect) were prescribed. For the future climate (2001-2100) these concentrations were prescribed according to three different IPCC scenarios (B1, A1B, B2).

In our study over South Africa we focus on a control period representing current climate from 1961-1990, and on a future period representing a possible climate in the end of the 21st century from 2071-2100. Special attention is paid to changes of the hydrological cycle over large hydrological regimes. Thus, we are focusing on some major river systems in the southern African region located from north to south: Congo river, Zambezi river and Orange river (see Fig. 1). In addition, past changes in the region were analysed by considering observations, re-analysis data and downscaled re-analysis data using the regional climate model REMO.

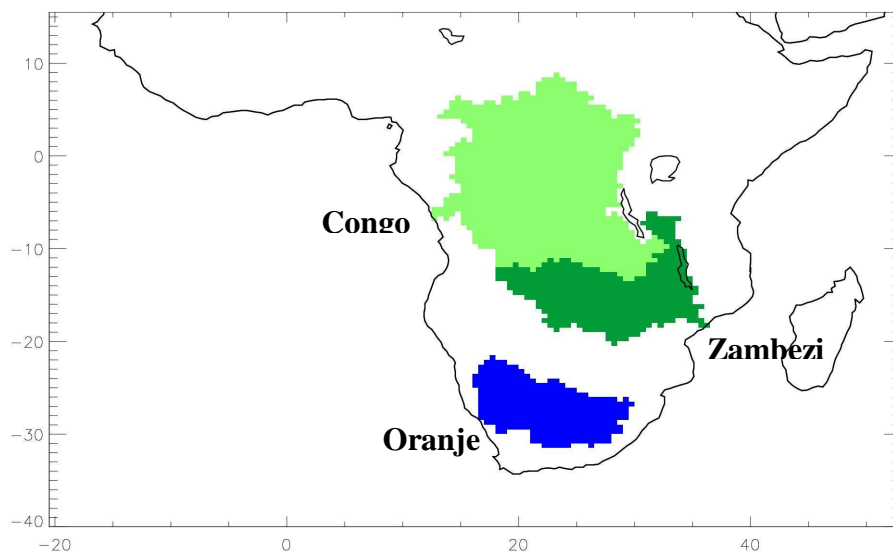


Fig. 1. Catchments of Congo, Zambezi and Orange river at 0.5 degree resolution

The results from the ECHAM5/MPI-OM IPCC simulations show a projected gradient in the climate change signal in the hydrological cycle over southern Africa for all three scenarios (see Fig. 2). A severe future drying is projected for the Oranje catchment (about -20% for precipitation, -50% for runoff), a moderate drying for the Zambezi catchment (about -7% for Precipitation, -15% for Runoff), and an enhancement of the hydrological cycle is projected for the Congo catchment (about +10% for precipitation, evaporation and runoff for A1B and A2, about + 6% for B1). The drying in the southern parts leads to less evaporation and intensifies the warming of the area.

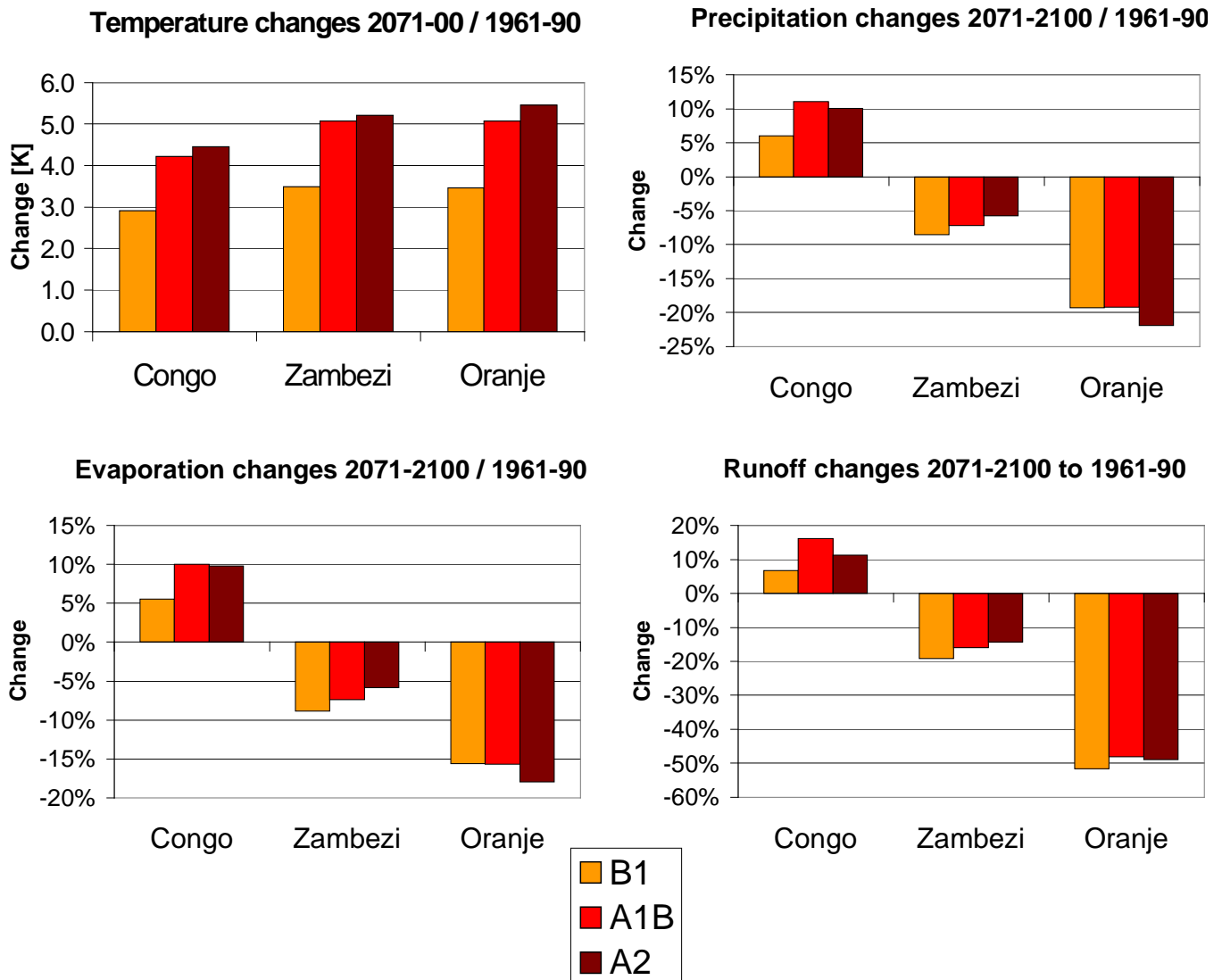


Fig.2. Projected changes (2071-2100 compared to 1961-1990) in the hydrological cycle over the Congo, Zambezi and Oranje river catchments.

Analysis of open water and loose ice areas in the Siberian Arctic from model simulations

V.Ch. Khon¹, I.I. Mokhov¹, E. Roeckner²

¹A.M. Obukhov Institute of Atmospheric Physics RAS, Moscow, Russia

²Max-Planck Institute for Meteorology, Hamburg, Germany
(khon@ifaran.ru)

Analysis of sea ice conditions affecting the duration of summer navigation through the Siberian Arctic seas (the North Sea Route) was performed using simulations with global climate model ECHAM5/MPI-OM (Marsland et al., 2003; Roeckner et al., 2003) with the SRES A2 scenario (IPCC, 2001). Characteristics of open water and loose ice (area, duration, dates of formation and freezing) for the warm season are analyzed. Daily sea ice concentration was used for detecting areas of open water and loose ice. We defined areas of open water and loose ice as areas with sea ice concentrations less than 10 % and 50 %, respectively (see Kern et al., 2005). Results of model simulations are compared to the ERA-40 reanalysis data (Simmons et al., 2000) for the period 1981-2000.

Figure 1 shows duration of loose ice for the warm season according to reanalysis (a) and model simulations (b) for the period 1981-2000. Model results show good agreement for loose ice duration in the Kara Sea. There are areas of less duration of loose ice in the Eastern Siberian Arctic (especially for East-Siberian and Chukchi Seas) in comparison with reanalysis.

Figure 1. Mean duration (in days) of summer loose ice (< 50 % sea ice concentration) in warm season according to the ERA-40 reanalysis (a) and model simulations with ECHAM5/MPI-OM (b) for the period 1981-2000.

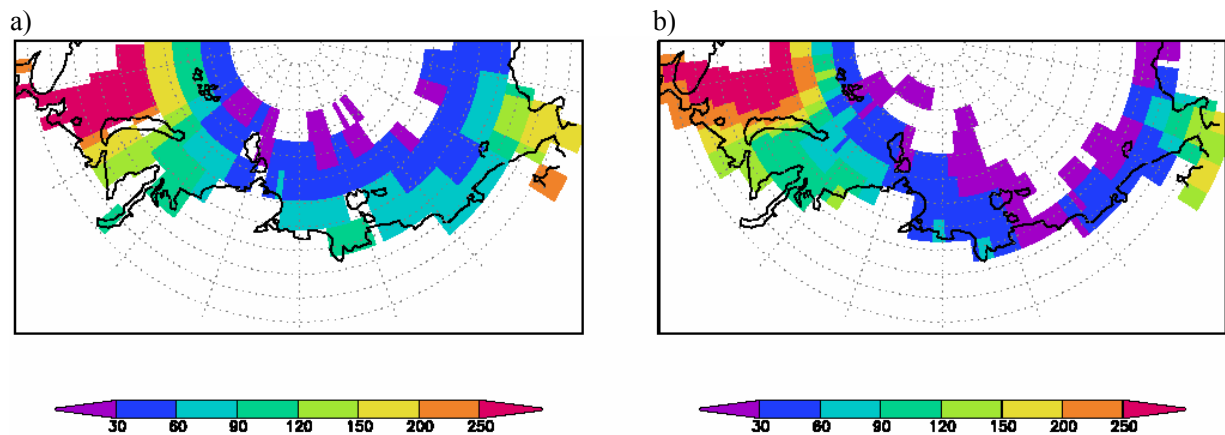


Figure 2 demonstrates trends of open water (a) and loose ice (a) duration in warm season according to model simulations for the period 2001-2050. Figure 3 shows mean area (in %) of open water and loose ice in the Kara (a) and Laptev (b) Seas for the different 10-years periods (1991-2000, 2021-2030, 2051-2060, 2081-2090) of model simulations. According to model results an increasing of the open water and loose ice area in the Kara Sea is connected with earlier ice melting and later ice freezing in the XXI century.

Figure 2. Trends (in days per 50 years) of open water (a) and loose ice (b) duration in warm season according to model simulations (SRES A2) for the period 2001-2050.

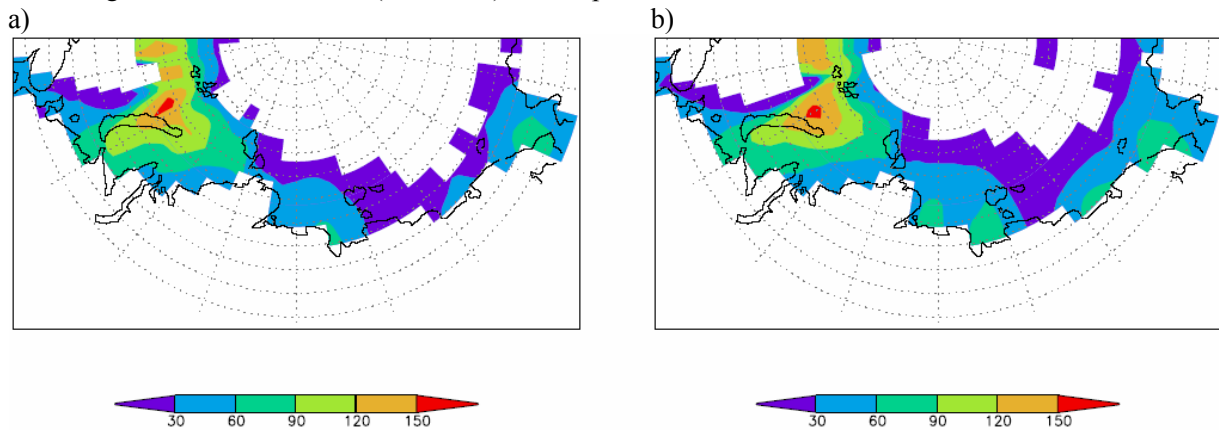
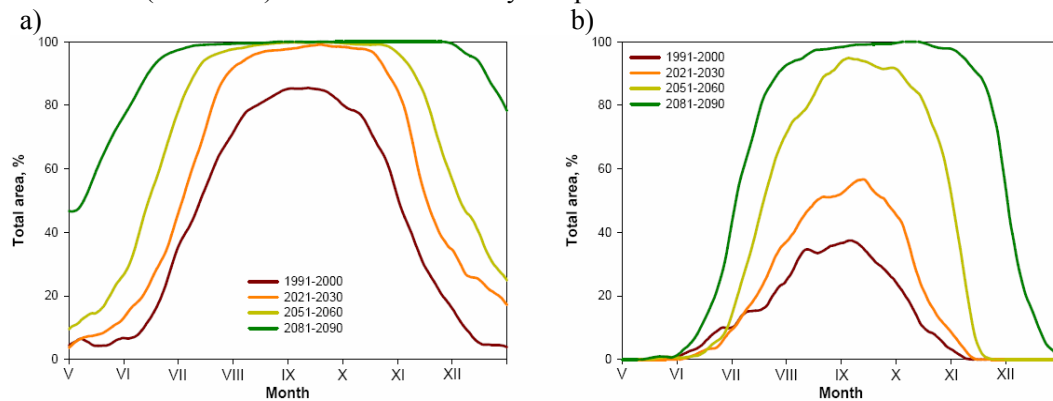


Figure 3. Mean area (%) of open water and loose ice in the Kara (a) and Laptev (b) Seas according to model simulations (SRES A2) for the different 10-years periods.



For the Laptev Sea model results show the increase for intensity of loose ice formation with a tendency to later ice freezing in the XXI century.

This study was supported by the RFBR and RAS program.

References

- Climate Change 2001: The Scientific Basis. Intergovernmental Panel on Climate Change. J.T. Houghton, Y. Ding, D.J. Griggs et al. (eds.), Cambridge Univ. Press. Cambridge, 881p.
- Kern, S., I. Harms, S. Bakan, and Y. Chen (2005), A comprehensive view of Kara Sea polynya dynamics, sea-ice compactness and export from model and remote sensing data, *Geophys. Res. Lett.*, 32, L15501, doi:10.1029/2005GL023532.
- Marsland, S. J., H. Haak, J. H. Jungclaus, M. Latif, and F. Röske, 2003: The Max-Planck-Institute global ocean/sea ice model with orthogonal curvilinear coordinates. *Ocean Model.*, 5, 91–127.
- Roeckner E., Bäuml G., Bonaventura L., Brokopf R., Esch M., Giorgetta M., Hagemann S., Kirchner I., Kornbluh L., Manzini E., Rhodin A., Schlese U., Schulzweida U., Tompkins A. The atmospheric general circulation model ECHAM 5. Part I: Model description / MPI Rep. 349, Max Planck Institute for Meteorology, Hamburg. 2003.

Regional Climate Model sensitivity to domain size

Martin Leduc and René Laprise
Canadian Regional Climate Modelling Network
Université du Québec à Montréal (leduc@sca.uqam.ca, laprise.rene@uqam.ca)

1 Introduction

Regional Climate Models are increasingly used to add small-scale features that are not present in their lateral boundary conditions (LBCs). It is well known that the computational domain of RCMs must be large enough to allow the development of small scales (Jones et al., 1995). On the other hand, integrations on very large domains have shown important departures from the driving data, unless large-scale nudging is applied (e.g., Castro and Pielke, 2005).

Here the effects related to the domain size will be examined using the "Big-Brother" approach developed by Denis et al. (2002a).

2 Experimental framework

The Canadian Regional Climate Model (CRCM; Caya and Laprise, 1999) is first driven by NCEP reanalyses to simulate a winter-month, the Big Brother (BB) as illustrated on Fig. 1. A low-pass filter based on discrete cosine transform (DCT; Denis et al., 2002b) that retains all wavelengths longer than 2160 km and removes those smaller than 1080 km (with a gradual

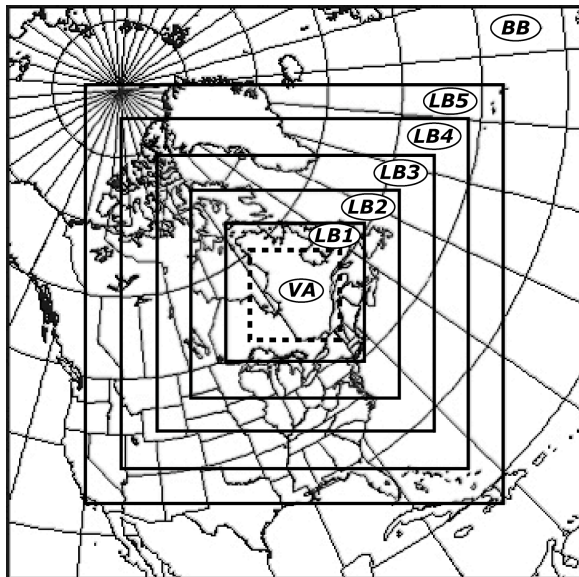


Fig. 1 Domain sizes used for simulations LB1 to LB5, and BB, the reference. Statistics are computed on the VA window.

transition in between) is then applied on this dataset to emulate coarse-resolution LBC that are usually taken from GCMs or reanalyses. These data are then used to drive five simulations called the "Little Brothers" (LB1 to LB5 on Fig. 1) with different grid sizes but centred on the same location. The DCT decomposition is applied on the five LB simulations to separate the large (nested) and small (added) scales. Climate diagnostics of the various LB are compared to those of the BB over the verification area noted VA on Fig. 1.

3 Results

The temporal correlation, variance ratio and normalized mean-square difference are summarized on a Taylor diagram (Taylor, 2001). Fig. 2a displays the results for the large-scale component of the 850-hPa geopotential height. All LB simulations have excellent variance ratios, with a slight underestimation for the largest domains LB4 and LB5. The temporal correlation of the large scales improves slightly when the LB domain is reduced from 144x144 to 72x72, but little when further reduced to 48x48.

A reduction of the mean-square error is also noted for fields such as temperature (not shown) when the domain is made smaller. More turbulent fields such as vorticity or relative humidity (not shown) also exhibit similar behaviours at large scales; a difference with fields such as geopotential and temperature, however, is a small loss of correlation (4%) when passing from LB2 to the smallest domain size LB1. All these comments on large scales also apply to the fields at 700 hPa.

The statistics for the small-scale component of the 850-hPa geopotential height are shown on Fig. 2b. There is a continuous gain of correlation in shrinking domain size from LB5 to LB2. When compared to Fig. 2a, correlation improvements suggest that consistence of small-scale features is in some way helped by the increased correlation in the large-scale flow.

Fine-scale statistics are affected differently when reducing the domain size beyond 96x96. Normalized mean-square difference stops to reduce at a grid size of 72x72, and shows a

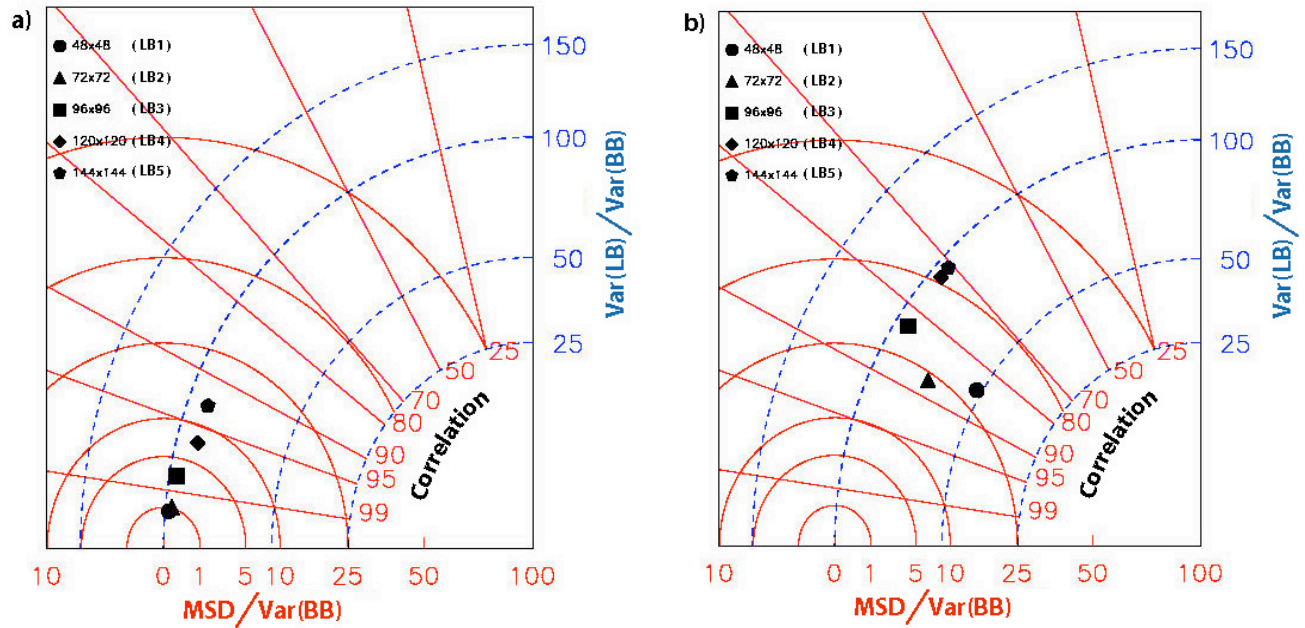


Fig. 2 Taylor diagrams for the transient component of 850-hPa geopotential height, showing the mean-square difference, temporal correlation and variance ratio for (a) large scales (driven) and (b) small scales (added). The three quantities are normalized by and compared with the Big Brother values.

subtle increase for the smallest domain. It is worth noting that an important underestimation of variance occurs when the domain size is reduced beyond 96x96. Other fields such as relative humidity and vorticity (not shown) exhibit similar behaviours when the domain is reduced. Temperature (not shown) exhibits large variance under-estimation for the smallest domain LB1 (66.0%) only, while the four other simulations stay between 82% and 91% of the BB's variance. At 700 hPa, the analysis (not shown) reveals an even larger variance underestimation for the three smallest domains. Since winds are stronger at this level, it suggests that small-scale features are advected out of the domain area before they have time to fully develop.

4 Conclusions

Driven (large) and added (small) scales in simulations of an RCM using different domain sizes were studied. Large scales show some sensitivity to the domain size, with best results for smaller domains, owing to the better control exerted by LBC. Some underestimation of the large-scale variance was noted for the two larger domains. This fact seems to be consistent with large-scale kinetic energy underestimation observed by Castro and Pielke (2005).

Two effects of domain-size reduction were observed on the small-scale component of

fields. The temporal correlation improves when reducing domain sizes from LB5 to LB2. This improvement in small scales appears to be linked to the better control of the large scales in smaller domains. But temporal variance is largely underestimated when the domain becomes smaller than 96x96, particularly at higher levels. This loss can be partly explained by considering the period that small scales need to develop sufficiently and the time scale of the ventilation through the domain by the large-scale flow. This phenomenon is most clearly visible on variance-ratio maps (not shown) where low values are in general distributed along the inflow boundary.

5 References

- 1- Caya, D., and R. Laprise, 1999: A semi-implicit semi-Lagrangian regional climate model: The Canadian RCM. *Monthly Weather Review*, 127, 341-362.
- 2- Castro, C.L., and R.A. Pielke, 2005: Dynamical Downscaling: Assessment of Value Retained and Added Using the Regional Atmospheric Modeling System (RAMS). *Journal of Geophysical Research* (submitted) 1-66.
- 3- Denis, B., R. Laprise, D. Caya and J. Côté, 2002a: Downscaling ability of one-way nested regional climate models: The Big-Brother experiment. *Climate Dynamics*, 18, 627-646.
- 4- Denis, B., J. Côté and R. Laprise, 2002b: Spectral decomposition of two-dimensional atmospheric fields on limited-area domains using the discrete cosine transform (DCT). *Monthly Weather Review*, 130, 1812-1829.

Relation between RCM's internal variability and residency time of the atmospheric parcels into the limited area domain

Philippe Lucas-Picher¹, Daniel Caya² and Sébastien Biner²

¹Department of Environmental Sciences, UQAM, Montréal, Québec, Canada. (picher@sca.uqam.ca)

²Ouranos Consortium, Montréal, Québec, Canada.

Internal variability is an intrinsic characteristic of the climate system. It is the variability in the climate system that is observed without modification in the forcings. This variability comes from the dynamic and thermodynamic non-linear relations which govern the atmosphere and oceans circulations. This variability is also generated by the interactions between the components of the climate systems, which operate at different time scales.

The internal variability in general circulation models (GCM) is visible when two simulations started with different initial conditions diverge from one another leading to two completely different states after few days. In regional climate models (RCM), internal variability is still present but usually lower than GCM's one because the RCM domain is limited and a continual flow of information, which feeds the limited area domain at the boundaries, controls the simulation.

Lucas-Picher et al. (2004) showed that RCM's internal variability increases with domain size due to the weakening of the lateral forcing as the domain expand. Rinke et al. (2004) demonstrated that the RCM's internal variability in an Arctic domain is higher than one in the mid-latitude due to the weak atmospheric flow through the boundaries of the RCM over the Arctic which limits the flow of new information in the domain. The purpose of this work is to study the relation between the residency time of the atmospheric parcels into the limited area domain and the amplitude of the internal variability in RCMs.

To look at the internal variability, two ten-year simulations (1980-1989) are started with a one-month lag in their initial conditions using the Canadian Regional Climate Model (CRCM) (Caya and Laprise, 1999). The CRCM simulations are driven by NCEP reanalysis over a domain of 193 by 145 grid points at 45-km resolution. An ageing tracer is used to evaluate the residency time of each atmospheric parcel into the limited area domain. The tracer works as a pollutant

atmospheric tracer where the concentration is replaced by the time spent in the domain. When an atmospheric parcel comes into the domain, its tracer is initialized to 0 and at every time step, the tracer is ageing 15 minutes. The tracers are fully advected by the model circulation.

Figure 1 shows the mean summer and winter residency time at 850 hPa for the ten-year simulation. Because of the westward general circulation, the time spent in the domain is shorter on the west side of the domain than on the east side. According to the faster circulation in winter, the residency time is shorter in winter than in summer. The residency time over the Rocky Mountains and Greenland have to be ignored because a simple interpolation is done through the mountains to get the values at 850 hPa. These values will be masked in the subsequent analysis.

The internal variability is measured from the differences between each lagged simulation using the temporal root mean square difference (TRMSD):

$$TRMSD(i, j, k) = \sqrt{\frac{1}{NT} \sum_{t=1}^{NT} (A(i, j, k, t) - B(i, j, k, t))^2},$$

where A and B are the two simulations and NT is the length of the simulation in number of time steps. Figure 2 presents the TRMSD of mean sea level pressure (MSLP) for summer and winter. The summer and winter figures are similar. On the western side of the domain, the differences between each simulation are low because the atmospheric flow just came into the domain. At the opposite, on the eastern side of the domain, the differences are high because the simulations have time to diverge from one another and the lateral forcing is weak.

To study a relation between the residency time and the MSLP TRMSD, a scatter plot using each cells of the domain is drawn (see fig. 3). On each plot, the best linear fit is drawn and the equation of this fit is indicated. Also, the linear correlation is computed. The cloud of points exhibits approximately a linear fit where small

TRMSD have a short residency time and high TRMSD have a long residency time. The correlation between the residency time and the TRMSD is of 0.94 in summer and winter, meaning that the relation is strong. With the same pattern of TRMSD, it is the slope of the fit that differentiate the summer from the winter. For a same residency time, each simulation has higher differences in winter than in summer. This can be explained by the stronger gradients in winter where different behavior for each simulation created large differences. This is a preliminary study and it is expected that this relation will not be present for all atmospheric variables.

References

- Caya, D. and R. Laprise, 1999: A semi-implicit semi-Lagrangian regional climate model: The Canadian RCM, *Mon. Wea. Rev.*, 127 (3), 341-362.
- Lucas-Picher, P., D. Caya and S. Biner, 2004: RCM's internal variability as function of domain size. *Research activities in Atmospheric and Oceanic Modelling*, WMO/TD, J. Côté, Ed., 1220 (34): 7.27-7.28.
- Rinke, A., P. Marbaix and K. Dethloff, 2004: Internal variability in arctic regional climate simulations: Case study for the SHEBA year, *Climate research*, 27, 197-209.

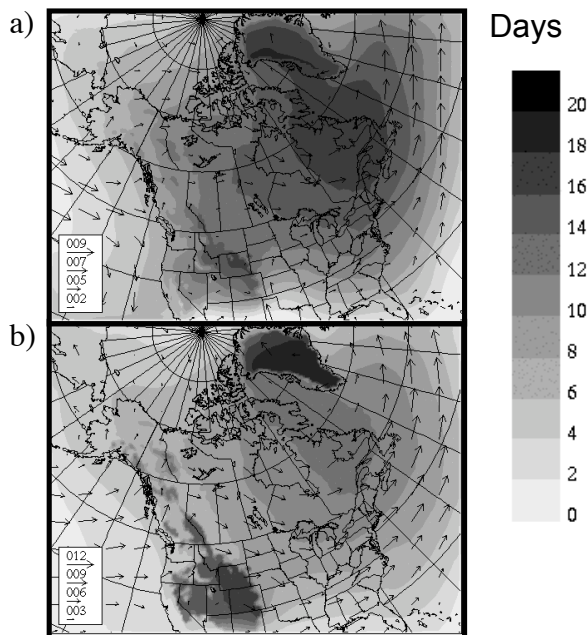


Figure 1. Mean residency time in a) summer (JJA) and b) winter (DJF) at 850 hPa for the ten-year simulation. The arrows indicate the wind circulation.

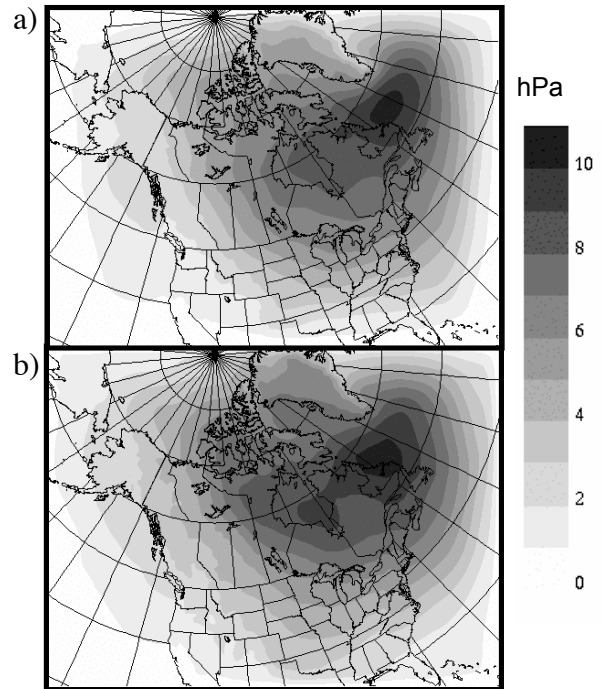


Figure 2. MSLP TRMSD for a) summer (JJA) and b) winter (DJF) for the ten-year simulation.

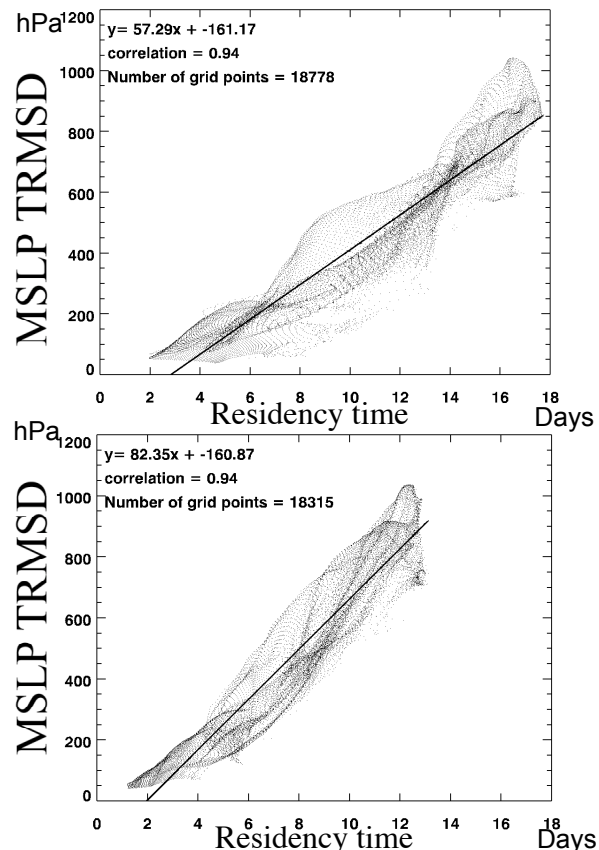


Figure 3. Scatter plot between the MSLP TRMSD and the residency time in a) summer (JJA) and b) winter (DJF).

Analysis of relationship between the Arctic climate and intensity of thermohaline circulation from model simulations

Mokhov I.I.¹, Artamonov A.Yu.^{1,2}, Bezverkhny V.A.¹, Karpenko A.A.¹, Muryshev K.E.^{1,2}, Khon V.Ch.¹, Roeckner E.³

¹A.M. Obukhov Institute of Atmospheric Physics RAS, Moscow, Russia

²Moscow Institute for Physics and Technology, Russia

³Max-Planck Institute for Meteorology, Hamburg, Germany

mokhov@ifaran.ru

Relationships between intensity of thermohaline circulation I_{THC} in the North Atlantic and Arctic climate characteristics are studied. The analysis is based on the ECHAM5/MPI-OM general circulation model simulations (Marsland et al., 2003; Roeckner et al., 2003) with the SRES B1 scenario (IPCC, 2001) for 2001–2100 and with the greenhouse gases concentrations in the atmosphere (GHG) from observations for 1860–2000. Different methods are used including two methods of cross-wavelet analysis (CWA): CWA-1 (Bezverkhny, 2001; Mokhov et al., 2005) and CWA-2 (Jevrejeva et al., 2003; Grinsted et al., 2004).

Figure 1 shows coefficients of correlation r between the I_{THC} and averaged over the Arctic and sub-Arctic latitudes (60-90N) surface air temperature T_A (a), salinity S_A (b) and total sea ice area in the Arctic Ocean I_A (c) for 100-year moving intervals. According to Fig.1 correlation between I_{THC} and S_A is always positive with a general increase from about $0.2 \div 0.35$ in the 19th-20th to about 0.7 and later decrease to 0.6 in the 21st century. Correlation between I_{THC} and T_A changes the sign from the relatively low positive values to the negative values growing by absolute value and then stabilizing at the level about -0.65. The correlation between I_{THC} and I_A is almost symmetric relative 0 in comparison to the correlation between I_{THC} and T_A . It is related to the strong negative correlation between T_A and I_A with the increase of r from about -0.8 in the 19th-20th centuries to about $-(0.98 \div 0.99)$ in the 21st century. Correlation between I_{THC} and Siberian rivers runoff was also analyzed but this correlation is quite weak with maximum r about 0.2 by absolute value.

Corresponding correlation analysis with shorter moving intervals (with 50- and 30-year moving intervals, in particular) shows more unsteady evolution of relationships. Even more complicated dynamics of relationships displays CWA. Coherency of I_{THC} and S_A is different for various periods and changes essentially in time. In particular, significant changes were noted for coherency and phase lags between I_{THC} and S_A for variations with periods about 20-50 years at the end of the 20th century and in the 21st century (especially in its first half) both with CWA-1 and CWA-2. Differences were obtained for variations with periods larger and smaller than 20-30 years.

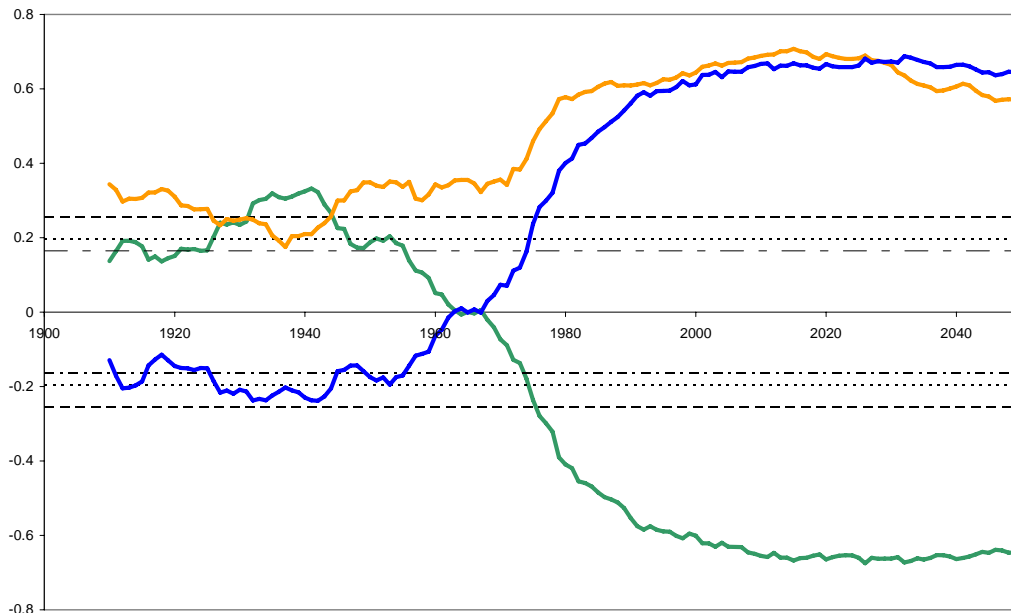
According to this analysis phase lags between I_{THC} and characteristics of the Arctic climate can be of different sign for various periods of variations. In particular, it was noted that variations of T_A can lead variations of I_{THC} at periods about 30 years while can lag at periods about 60 years.

This study was supported by the RFBR and RAS program.

References

- Bezverkhny, V.A., 2001: Developing the wavelet-transform method for analysis of geophysical data. *Izvestiya, Atmos. Oceanic. Phys.*, **37**, No. 5, 584-591.
- Climate Change 2001: The Scientific Basis. Intergovernmental Panel on Climate Change. J.T. Houghton, Y. Ding, D.J. Griggs et al. (eds.), Cambridge Univ. Press. Cambridge, 881p.
- Grinsted, A., J.C. Moore, and S. Jevrejeva, 2004: Application of the cross wavelet transform and wavelet coherence to geophysical time series. *Nonlin. Proc. Geophys.*, **11**, 561-566.
- Jevrejeva, S., J. Moore, A. Grinsted, 2003: Influence of the Arctic Oscillation and El Niño – Southern Oscillation (ENSO) on ice conditions in the Baltic Sea: The wavelet approach. *J. Geophys. Res.*, **108** (D21), 4677, doi:10.1029/2003JD003417.
- Marsland, S. J., H. Haak, J. H. Jungclauss, M. Latif, and F. Röske, 2003: The Max-Planck-Institute global ocean/sea ice model with orthogonal curvilinear coordinates. *Ocean Model.*, **5**, 91–127.
- Mokhov, I.I., V.A. Bezverkhny, A.A. Karpenko, 2005: Diagnosis of relative variations in atmospheric greenhouse gas contents and temperature from Vostok Antarctic ice core paleoreconstructions. *Izvestiya, Atmos. Oceanic. Phys.*, **41**, No.5, 523-536.
- Roeckner E., Bäuml G., Bonaventura L., Brokopf R., Esch M., Giorgetta M., Hagemann S., Kirchner I., Kornbluh L., Manzini E., Rhodin A., Schlese U., Schulzweida U., Tompkins A. The atmospheric general circulation model ECHAM 5. Part I: Model description / MPI Rep. 349, Max Planck Institute for Meteorology, Hamburg. 2003.

Figure 1. Coefficients of correlation between THC intensity I_{THC} and climate characteristics for the Arctic region (60-90N) (for 100-year moving intervals): surface air temperature T_A (a), salinity S_A (b) and sea ice area I_A (c). Horizontal lines show minimum values of coefficients of correlation necessary for statistical significance at the 90, 95 and 99% level.



Dynamical Downscaling with ECMWF Seasonal Forecasts

Mirta Patarčić and Čedo Branković
Croatian Meteorological and Hydrological Service
patarcic@cirus.dhz.hr
cedo.brankovic@cirus.dhz.hr

The principal aim of seasonal forecasting is to predict the range of values that is most likely to occur during the next season. Seasonal forecast information can be used for decision making in, for example, agriculture, water resources management, production of electricity, etc. It can also help alleviating the effects of extreme climate fluctuations such as droughts and floods.

General circulation models make seasonal forecasts at spatial scales of the order of hundreds of kilometres without actually revealing details in surface fields that depend on orography, such as precipitation or surface temperature. One method of increasing the spatial and temporal resolution of the fields of interest is to dynamically downscale the output of global models by using regional climate models.

In this study we used the Regional Climate Model (RegCM; Giorgi et al. 1993) to downscale ECMWF operational seasonal forecasts for the summer (June-August) of 2003. The ECMWF model resolution was T_L95 , approximately corresponding to 1.875° on the quasi-regular grid. The input fields for RegCM have been taken from the ECMWF seasonal forecast archive – only fields at six standard pressure levels (1000, 925, 850, 700, 500 and 200 hPa) with the 12-hour frequency were available. In order to reduce computational requirements for downscaling the whole ECMWF seasonal forecasts ensemble (40 integrations), a subset of seasonal forecasts has been made by applying Ward's hierarchical clustering technique (Anderberg, 1973). For a given area, those members that explain 50% of the ensemble variance have been selected. For the clustering purpose, monthly means of 500 hPa geopotential heights for the first and second summer month (June and July) in 2003 have been retrieved from ECMWF seasonal forecast archive. The common members from the most populated clusters in each month were selected, thus resulting in 12 seasonal forecasts to be downscaled. The RegCM domain covered the central and southern Europe and the northern Mediterranean and the model horizontal resolution was set to 50 km. The model top was at 200 hPa with 14 vertical levels.

In order to determine the differences between the fields after downscaling, the RegCM seasonal ensemble means have been compared with the sub-ensemble seasonal means of the ECMWF model. ECMWF sub-ensemble seasonal means have been retrieved at $2^\circ \times 2^\circ$ lat/lon grid for the same 12 members used for downscaling.

The benefits of the denser grid can be clearly seen from Figure 1. showing the total precipitation seasonal mean for (a) RegCM seasonal forecasts ensemble and (b) ECMWF model sub-ensemble mean. While the ECMWF model seasonal mean indicates increased precipitation in the Alpine region, the RegCM seasonal mean clearly gives more detailed structure over the Alps, the Carpathian Mountains, the Balkan Peninsula, the Pyrenees and the Atlas Mountains on the border of the integration domain. The

difference between RegCM and ECMWF precipitation averages is not negligible – in both coastal and continental parts of Croatia it amounts between 1 and 3 mmday^{-1} . RegCM proved to be very robust despite such a poor input from the ECMWF operational archive. It is therefore hoped that with more levels and more frequent time intervals even better downscaling result would have been achieved.

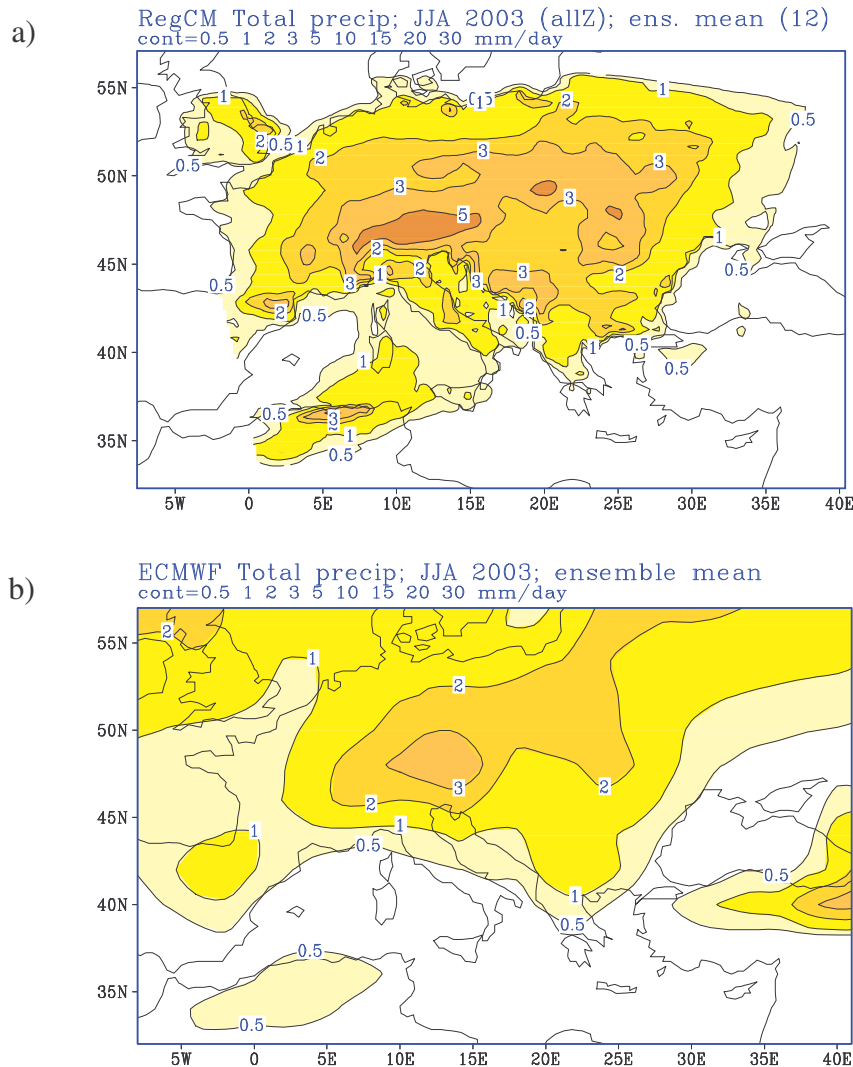


Figure 1. The JJA 2003 total precipitation ensemble mean (mmday^{-1}) for a) RegCM and b) ECMWF model. Contouring: 0.5, 1, 2, 3, 5, 10, 15, 20, 30 mmday^{-1} .

References:

Anderberg, M.R., 1973: Cluster analysis for applications. Academic Press, New York.

Giorgi, F., Marinucci, M.R. and Bates, G.T. , 1993: Development of a second-generation regional climate model (RegCM2), Part I: Boundary-layer and radiative transfer processes, *Monthly Weather Review*, 121, 2794-2813.

Seasonal Dynamical Downscaling for Crop Yield Estimation

D. W. Shin, J. G. Bellow, S. Cocke, T. E. LaRow, and James J. O'Brien
Center for Ocean-Atmospheric Prediction Studies, Florida State University, Tallahassee, FL, USA
(shin@coaps.fsu.edu)

This study describes the significant role of the CLM2 (Bonan et al. 2002) in the seasonal dynamical downscaling of surface fields (maximum and minimum temperatures, precipitation, and solar radiation) through the FSU regional climate model and explores the suitability of these surface fields for crop yield estimations using the CSM CROPGRO-peanut model (Jones et al. 2003). Seasonal simulations for peanut growing season with the atmospheric regional model coupled to the CLM2 (FSUCLM; Shin et al. 2005) are compared to those with the control (FSUc, i.e., the original FSU model). Two convective schemes (SAS and RAS) are also employed in this comparison.

The importance of the land model was clearly shown in seasonally downscaled surface climate simulations (Figs. 1 and 2). Three fields (maximum and minimum temperatures and solar radiation), among four input fields for use in a crop model, were simulated close to the observed seasonal climate in the new land model setup. However, precipitation was not since the amount of rainfall is mostly determined by the convective scheme. Nevertheless, the new land model modulated latent heat fluxes (or evaporation) better and provided a slightly better seasonal rainfall amount with the SAS scheme. In spite of noticeable gaps between the observed and the model seasonal climates, the regional climate model with the CLM2 provided more accurate site- and year-specific seasonal surface climates suitable for the crop model use (Fig. 3), resulting in improved estimation of peanut development and yield (Fig. 4). The FSUCLM with the SAS scheme exhibited its potential for simulating the interannual variability of crop yields. However, a conclusive statement cannot be made at this stage of the study. More work needs to be done to evaluate the skill of the model and to determine if the model has similar skill during other seasons, different locations, or different crop types.

In order to build a firm bridge between the climate model and the crop model, the following must be studied. First, a method should be developed to correct the inaccurate model precipitation by some dynamical and/or statistical methods. Second, ensemble simulations are needed to have a statistically significant result. These will be used to make probabilistic forecasts of the crop yield. Third, a coupled ocean-atmosphere model should be used instead of the prescribed sea surface temperature to provide an actual seasonal forecast to drive the crop model. Finally, a coupled version of atmospheric and crop models should be developed to capture the nonlinear seasonal weather-yield interactions. A comparison study is also needed to measure the current skill levels of dynamical downscaling approach compared to the statistical/empirical methods.

Acknowledgements

Computations were performed on the IBM SP4 at the FSU. COAPS receives its base support from the Applied Research Center, funded by NOAA Office of Global Programs awarded to Dr. James J. O'Brien. Additional support is provided by the USDA, CSREES.

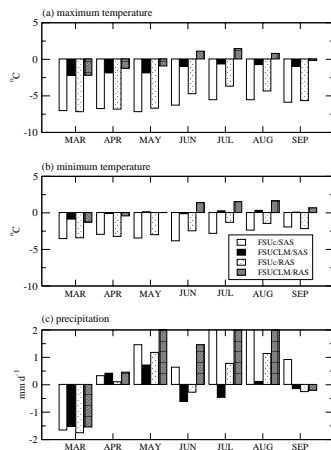


Fig. 1: Climatological (10-yr average) differences between model forecasts and the site-based observations for monthly mean (a) maximum temperature, (b) minimum temperature, and (c) rainfall amount. Values are averaged over the target states (FL, AL, and GA).

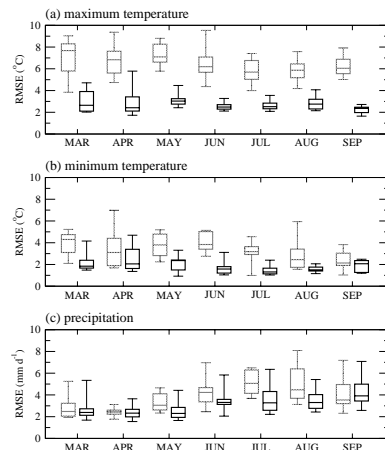


Fig. 2: Box-whisker diagrams of RMSE for monthly mean (a) maximum temperature, (b) minimum temperature, and (c) rainfall amount over the target states (FL, AL, and GA). The box shows the upper and lower quartiles, the line within the box shows the median and the whiskers show the full extent of the data (10 individual years). While gray boxes are for the FSUc/SAS, dark boxes are for the FSUCLM/RAS.

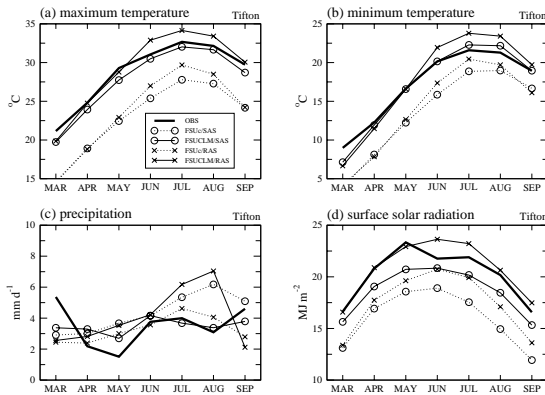


Fig. 3: Monthly mean (a) maximum temperature (°C), (b) minimum temperature (°C), (c) rainfall amount (mm d⁻¹), and (d) solar radiation (MJ m⁻²) for Tifton, GA from the climatology (10-yr average observation) and four corresponding model simulations.

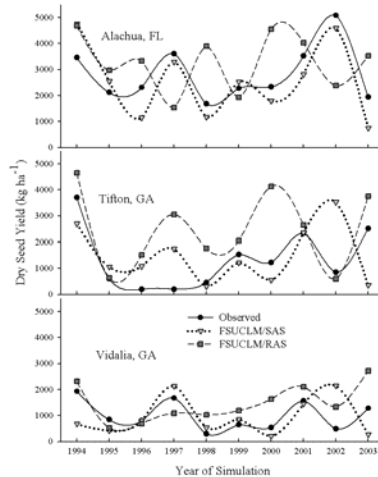


Fig. 4: Peanut (variety Georgia Green) yields from 1994 to 2003 simulated at three locations in the southeast U.S. using observed daily weather (circle) and the model daily values from the FSUCLM/SAS (triangle) and the FSUCLM/RAS (square).

References

- Bonan, G. B., K. W. Oleson, M. Vertenstein, S. Levis, X. Zeng, Y. Dai, R. E. Dickinson, and Z-L. Yang, 2002: The land surface climatology of the community land model coupled to the NCAR community climate model. *J. Climate*, **15**, 3123-3149.
- Jones, J. W., and co-authors, 2003: The DSSAT cropping system model. *Eur. J. Agron.*, **18**, 235-265.
- Shin, D. W., S. Cocke, T. E. LaRow, and J. J. O'Brien, 2005: Seasonal surface air temperature and precipitation in the FSU climate model coupled to the CLM2. *J. Climate*, **18**, 3217-3228.

Regional Climate Model for Siberia

Igor Shkolnik

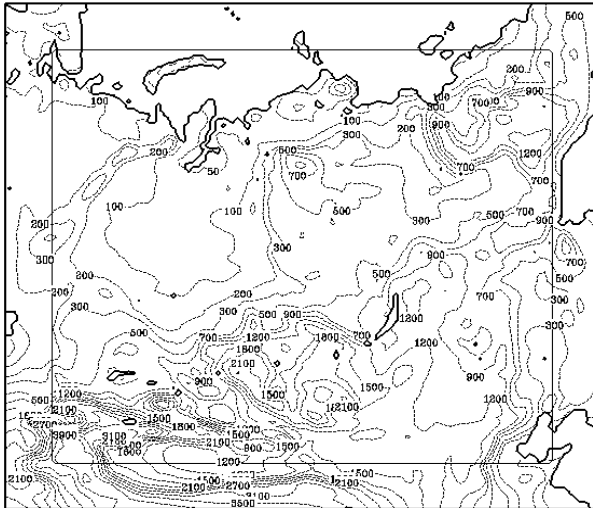
Voeikov Main Geophysical Observatory, Karbyshev str., 7, 194021, St. Petersburg, Russia

email: igor@main.mgo.rssi.ru

Introduction

According to observations the climate of Siberia has significantly changed over the last 50 years: the cold season by the end of 20th century has warmed by more than 4°C against the middle century climatology. The study is aimed at validation of the MGO RCM climatology over Siberian region (Fig.1), prior to simulation of future climate change. The MGO RCM is a primitive equation hydrostatic model currently run at 50 km resolution with domain size of 105×121 grid points. Physical package employed in the RCM is that of the MGO AGCM [<http://www-pcmdi.llnl.gov/projects/modeldoc/amip2/mgo-01a/mgo-01a.html>]. Previously the regional model was used for climate studies over the Western Russia and Central Europe [3,4]. The region of Siberia exhibits a number of specific features which can be summarized as follows:

- the regional climatology includes a broad range of climatic conditions from maritime to essentially continental; northern part of the region is an area of large atmospheric variability, while extended areas in the central and southern parts are poorly «ventilated»;



- the observational data necessary for model validation is very sparse and extremely irregular throughout the region;
- the region includes extended areas with complex and mountainous terrains; the modeling climatologies over these reveal most serious deficiencies;

Fig.1 The modeling domain and topography. The internal boundary of buffering subdomain is shown as rectangular.

Experiment and analysis

To assess modeling performance the NCEP/NCAR reanalysis [1] data at the lateral boundaries are used. The experimental setup is that used for the model validation over the western Russia described in [3]. The simulation period covers 6 years from 1982 to 1987 with lateral boundary conditions updated every 6 hours. Validation of the model simulated sea level pressure (SLP), surface air temperature (SAT), and precipitation (P) has been carried out against the reanalysis and analyses of SAT and P observations derived from CRU dataset [2] for respective years. The computed mean seasonal differences «model-reanalysis» for SLP revealed a good agreement between model and reanalysis indicating the Siberian High in winter and the Low in summer are reproduced by the model. Most of SLP biases are within the range of 0-3 hPa in winter (mostly positive) and 0-2 hPa in summer (mostly negative). The largest differences between the model and the reanalysis in winter occur over some areas in the central part of the domain where model simulated SLP is higher than the reanalysis by 5 hPa. In summer, the largest differences (up to -4 hPa) can be found over the eastern part. Some considerable biases occur in all seasons over mountains in the southern areas with elevations higher than 1500 m. Fig. 2ab shows winter and summer mean differences «model-CRU» for SAT. Also shown are the corresponding differences «reanalysis-CRU» for the same seasons (Fig.2cd). Both the model and reanalysis produce similar positive biases against CRU analyses in winter (larger than 4°C over the Lena and Yenisei river basins and southern Siberia). This implies a strong influence of lateral boundary forcing in winter on the RCM's internal energy balance limiting modeling skill in reproducing the analysed SAT. In summer, model biases are mostly within the range ±2°C with a tendency to slightly undersimulate SAT. The most noticeable cooling (by more than 4°C) was computed over mountains (this feature can be found in

all seasons). The summer cooling against CRU analysis is less pronounced in the reanalysis. In fig.2ef shown are winter and summer P differences. The computed P biases in both seasons are mostly within the reasonable range $\pm 30\%$ as compared against CRU analyses. The range is usually referred to as a measure of accuracy of the current models to reproduce water balance components at regional scale. However, in the presence of steep mountain slopes and complex terrain lacking representative observations, where agreement between modeled and analysed P distributions is less clear, the modeling errors can be beyond the indicated range. Temporal correlations of monthly mean SAT anomalies and monthly mean P with CRU analyses range from 0.5 to 0.98 and from 0.3 to 0.75, respectively. A somewhat higher correlation scores for P have been found over the areas with higher density of observing stations.

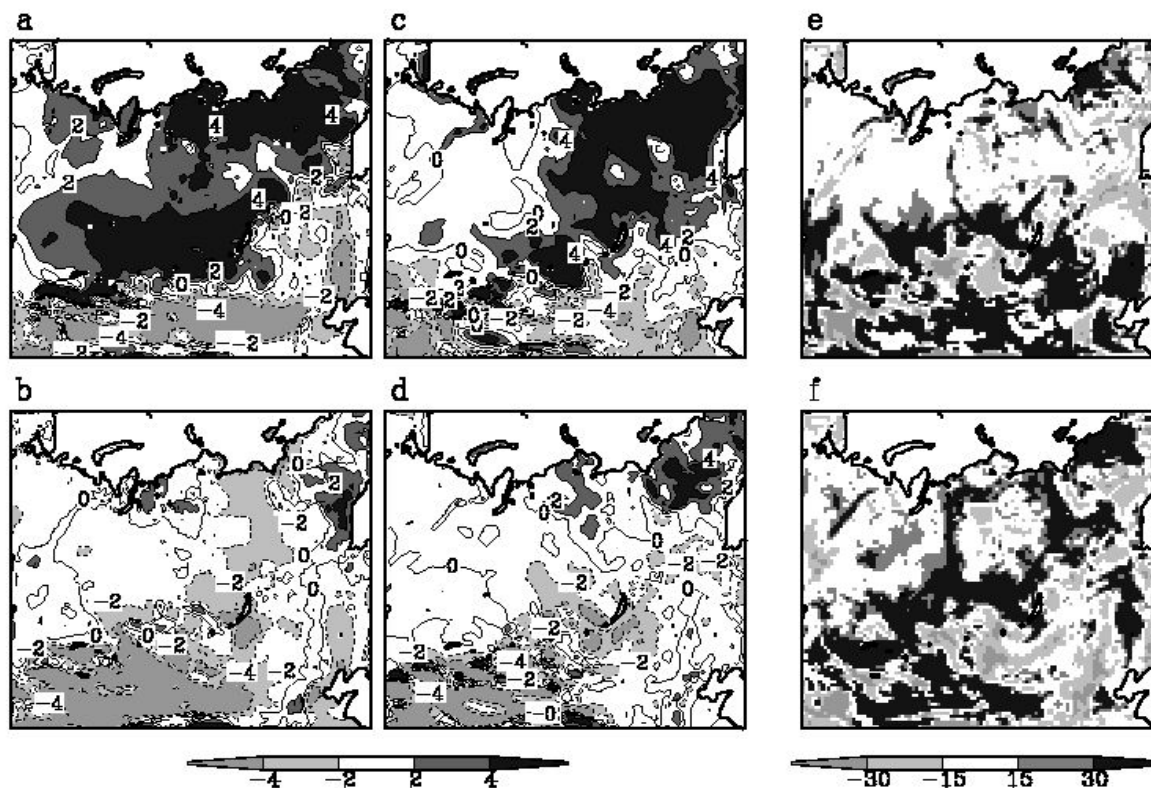


Fig.2 Differences ($^{\circ}\text{C}$) «model-CRU» and «reanalysis-CRU» for SAT in winter (a,c) and summer (b,d). The P differences (%) «model-CRU» are in the right column (e,f).

The work is supported by Russian Foundation for Basic Research (grants 04-05-08063-ofi_a, 06-05-64978-a, 06-05-64969-a). The plan is to further validate the RCM and simulate anthropogenic climate change using SRES A2 scenario over Siberian region.

References

1. Kalnay, E., Kanamitsu M., Kistler R., et al., 1996: The NCEP/NCAR 40-year Reanalysis Project. *Bull. Amer. Meteorol. Soc.*, 77, 437-471.
2. New M., Hulme M., and Jones P.D., 1999: Representing twentieth century space-time climate variability. Part I: Development of a 1961-1990 mean monthly terrestrial climatology. *J. Climate*, vol.12, pp. 829-856.
3. Shkolnik I.M., Meleshko V.P., Gavrilina V.M., 2005: Validation of the MGO regional climate model. *Russ. Meteorol. Hydrol.*, 1, pp. 14-27.
4. Shkolnik I.M., Meleshko V.P., Kattsov V.M., 2006: Climate change in the 21st century over the Western Russia: a simulation with the MGO Regional Climate Model. *Russ. Meteorol. Hydrol.*, 3, pp. 5-17.

SEASONAL DYNAMICAL DOWNSCALING WITH ERA-40 DATA

Lidija Srnec, Čedo Branković, Mirta Patarčić
Croatian Meteorological and Hydrological Service
srnec@cirus.dhz.hr, brankovic@cirus.dhz.hr, patarcic@cirus.dhz.hr

One of the main objectives for employing the Regional Climate Model (RegCM, Giorgi et al; 1993a,b) at the Croatian Meteorological and Hydrological Service (CHMS) is to dynamically downscale the operational seasonal forecasts of the European Centre for Medium-Range Weather Forecast (ECMWF). Since the ECMWF seasonal data archive contains only a limited amount of meteorological parameters available at a limited time frequency and at a restricted number of pressure levels, it was necessary to assess the sensitivity of RegCM to degrading forcing imposed by initial conditions (ICs) and lateral boundary conditions (LBCs). The testing has been done by using the following fields from ECMWF re-analysis data (ERA-40): surface pressure, geopotential height, temperature, u and v wind components and specific humidity.

In our experiments, the horizontal resolution was 50 km in an area of 60x50 grid points, centred over Croatia (at 45N, 16E). In the control experiment, the vertical number of levels was 18, extending from the surface to 100 hPa. The Lambert conformal projection was used. For the convection, the Grell scheme (Grell; 1993) was chosen with both Fritsch-Chappel (Fritsch and Chappel; 1980) and Arakawa-Schubert (Arakawa and Schubert; 1974) closures tested. First, we made changes in the ICs by increasing the horizontal resolution from T42 to T159. Then the LBCs were changed by reducing the frequency of updating from 6-hour to 12-hour intervals. Finally, changes in the model were introduced by lowering the top of the model from 100 to 200 hPa and reducing the number of vertical levels from 18 to 14. The details of the experimental design and the results are given in Branković et al. (2005).

Although the simulations have been carried out for the two seasons only (DJF 1993/94 and JJA 1997), the following can be concluded. The increase in the ICs and LBCs horizontal resolution reduces the geopotential, cools the upper-air and lower atmosphere and reduces the summer convective precipitation. The reduced frequency of the LBCs update mostly shows the opposite results, i.e. an increase in geopotential and temperature. When the top of the model is lowered, both upper and low level summer winds are strengthened. This effect is partly offset when the number of model levels is reduced. The changes in the vertical configuration cause on average much weaker effects on surface fields than the changes in LBCs. The Arakawa-Schubert closure reduces the amount of summer convective precipitation in the given domain when compared with the Fritsch-Chappel closure.

The verification of the model configuration closest to the seasonal forecasts archive (T159 horizontal resolution, 12-hourly updates with model top at 200 hPa and 14 vertical levels) against ERA-40 data shows that the model underestimates geopotential heights and low-level temperature, but overestimates temperature at upper levels (Fig. 1). The precipitation is overestimated over the central and southern parts of the integration domain (mainly over the mountains) when compared to the CRU observational data. These differences do not critically affect seasonal downscaling. The first experience with the RegCM in the CHMS is certainly encouraging and further testing and assessment of model integrations will be continued.

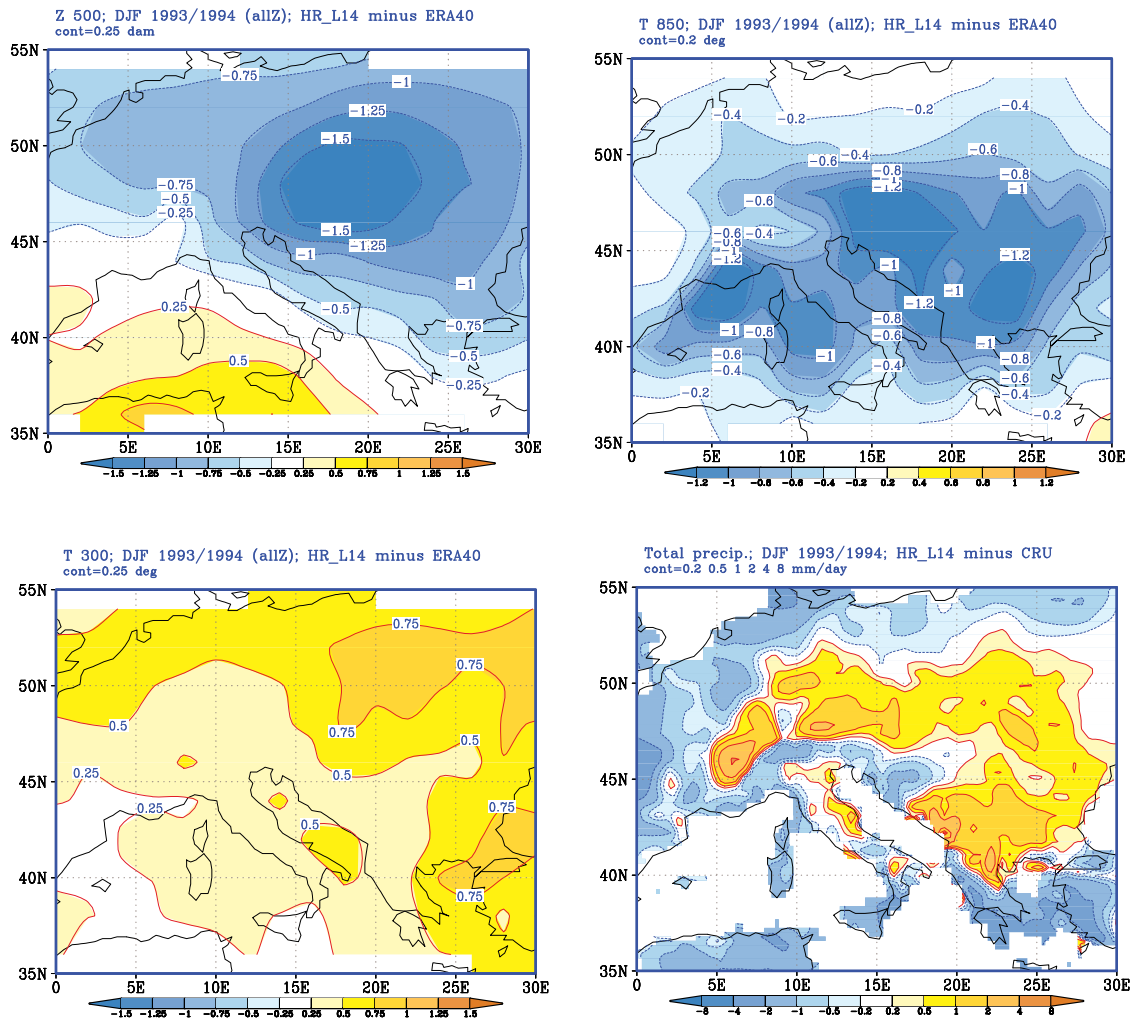


Figure 1. Verification of the RegCM experiment (T159 horizontal resolution, 12-hourly updates with model top at 200 hPa and 14 vertical levels) for DJF 1993/94: for 500 hPa geopotential height (top left), 850 hPa temperature (top right), 300 hPa temperature (bottom left) and total precipitation (bottom right). Contours for geopotential every 0.25 dam, for 850 hPa temperature 0.2 deg, for 300 hPa temperature 0.25 deg and for total precipitation at 0.2, 0.5, 1, 2, 4, 8 mmday⁻¹

References:

Branković, Č., M. Patarčić and L. Srnc, 2005: Seasonal dynamical downscaling with ERA-40 data: A sensitivity study. *Croatian Meteorol. J.*, 39, 15-39.

Fritsch, J.M. and C.F. Chappel, 1980: Numerical predictions of convectively driven mesoscale pressure systems. Part I: Convective parameterization. *J. Atmos. Sci.*, 37, 1722-1733.

Giorgi, F., M.R. Marinucci and G.T. Bates, 1993a: Development of a second-generation regional climate model (RegCM2), Part I: Boundary-layer and radiative transfer processes. *Mon. Wea. Rev.*, 121, 2794-2813.

Giorgi, F., G. De Canio and G.T. Bates, 1993b: Development of a second-generation regional climate model (RegCM2), Part II: Convective processes and assimilation of lateral boundary conditions. *Mon. Wea. Rev.*, 121, 2814-2832.

Grell, G.A., 1993: Prognostic evaluation of assumptions used by cumulus parameterizations. *Mon. Wea. Rev.*, 121, 764-787.

Precipitation forecast using a multi model superensemble and understanding its diurnal variability

T.N. Krishnamurti¹, C. Gnanaseelan^{1,2} and Arindam Chakraborty¹

¹Dept. of Meteorology, Florida State University
Tallahassee, FL 32306

²Indian Institute of Tropical Meteorology, Pune – 411008, India
[Email: tnk@io.met.fsu.edu]

Modelling the diurnal change of precipitation is a challenging scientific problem because the phase of the diurnal change varies quite a lot over the globe. This paper explores satellite data sets and the predicted precipitation from a suite of global coupled atmosphere ocean models to validate the phase and amplitude of the diurnal mode. The models are based on several versions of the FSU coupled global models that utilize different radiative transfer and cloud radiation schemes. These models differ in their prescription of cloud specifications. With these models we carry out a large sample of five-day forecasts. This study utilizes 3 hourly TRMM and model based data sets between 40°S and 40°N and highlights the advantage of constructing a superensemble for the forecasts of diurnal change since it reduces the large phase and amplitude errors of the member models.

The overall picture of afternoon rain over land areas and early morning rain over the ocean area are only partially true. Strong exception to this rule exists over many land and oceanic areas. Over the eastern Tibetan Plateau, during the northern summer season, afternoon showers are prevalent, however if we proceed 300 km to the southeast over the eastern foothills of the Himalayas the rainfall maximum occurs in the early morning hours. The aforementioned asymmetries within land or within ocean domain of the tropics suggests the possible complexity involved in the modelling of these features.

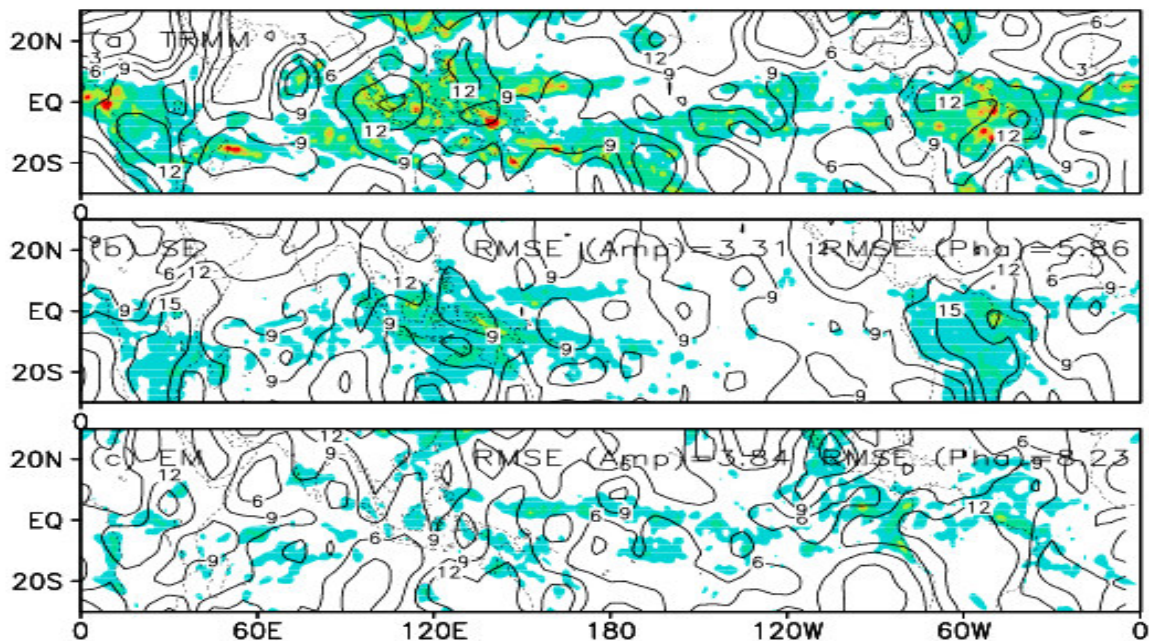


Fig. 1: Amplitude and phase (diurnal cycle) during 31 Mar–4 Apr 2000 (Day 5 forecast)

Figure 1 describes the amplitudes and phases of the diurnal cycle of the observed, superensemble and ensemble mean of the member models. The rms errors of the amplitude and phase of the diurnal modes predicted for day 1 of forecasts show that the phase of the superensemble is considerably better than those of other forecasts. The oceans generally carry a phase angle 06 and 09 hours local time (early morning). The land areas of South America and Africa carry a phase angle of around 15 to 18 hours (late afternoon). These features are best captured by the superensemble.

In figure 2 we show the equitable threat score for days 3 and 5 of forecasts. The results are similar for other days of forecasts. We include here the skills from the ensemble mean of the member models, those from a best model (that carries the lowest rms error for rainfall forecasts), those from a unified model (where a unified scheme for clouds is used) and those from the superensemble. The bar charts show the bias scores (close to 1.0 being a good score) along ordinate and the precipitation thresholds along the abscissa (i.e. Bias scores for rainfall totals greater than 2.5, 5, 10, 15, 20, 30, 40 and 50 mm/day). The right panels show the equitable threat score along ordinate plotted against the thresholds for rainfall totals. These illustrations show that the superensemble skills are the highest for all thresholds for precipitation forecasts for total rain up to 50 mm/day. The skill of the unified model, seen in the light of these probability skill measures, shows it to be superior to the best model for both the equitable threat score and the bias scores for most of the events. The best bias scores (closer to 1.0) are provided by the multi model superensemble.

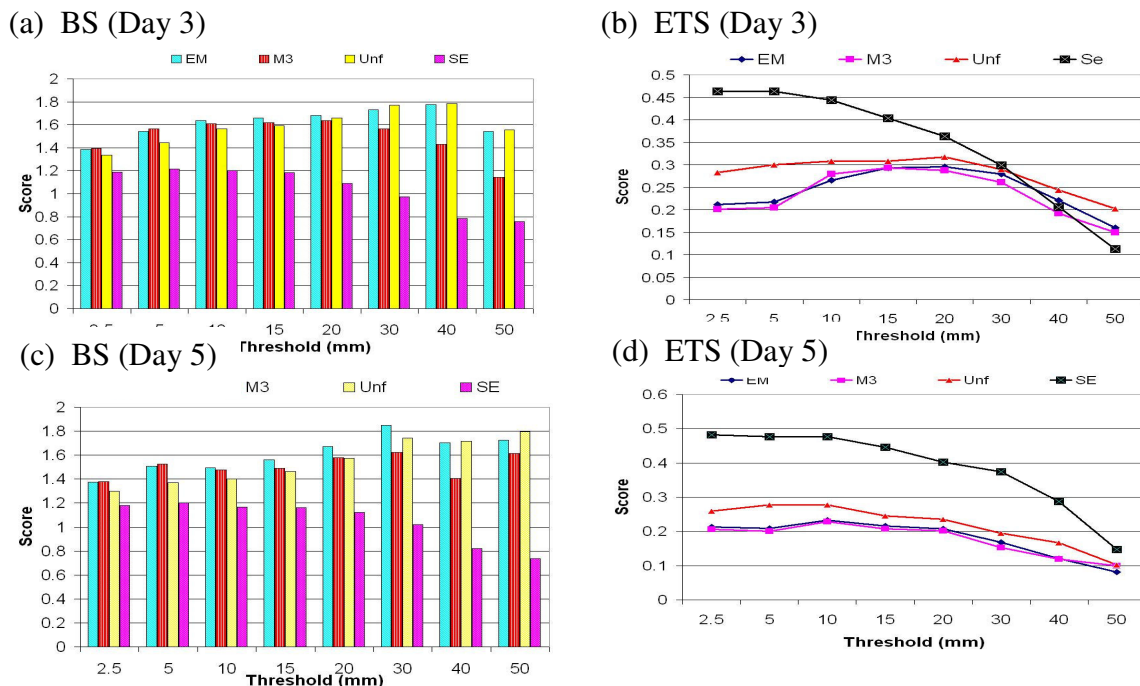


Fig. 2: The Bias Score (BS) [left panels] and Equitable Threat Score (ETS) [right panels] averaged over tropics, 0 to 360E, 30S to 30N during 29 Mar-02 Apr 2000 (Day 3 forecasts, top panels) and 31 Mar-04 Apr 2000 (Day 5 forecasts, bottom panels)

Sensitivity of model climate to physical parameterizations in climate models

Shuting Yang

Danish Meteorological Institute, Lyngbyvej 100, 2100 Copenhagen, Denmark

e-mail: shuting@dmi.dk

Different climate models usually give different atmospheric general circulation patterns that often differ considerably from observations. These differences in model climatology are associated with the differences in physics and numerics in climate models. However, due to the nonlinear nature and complexity of the models, it is difficult to identify the sources causing model deficiencies in the simulated climatology and variability. In order to attribute the model errors to specific modelling assumptions, many studies considered GCMs as being decomposed into modules that can be tested and compared independently. Held and Suarez (1994) proposed a benchmark calculation for evaluating the dynamical cores of GCMs independently of the physical parameterizations. Deque (1999) studied the intrinsic capacity of Eulerian and Semi-Lagrangian advection by using model configurations that only changed model dynamics while using the same physical parameterization package. Numerous efforts are also made to evaluate the parameterization schemes of specific physical process such as radiation (Ellingson et al. 1991; etc.) and land surface process (Henderson-Sellers et al. 1992).

In this study we investigate the influence of the physical parameterization as a whole package on model climatology. Two atmospheric climate models are used: the climate version of ARPEGE (v4) and the Danish climate model (DKCM). The atmospheric DKCM is developed at the Danish Meteorological Institute for applications in climate simulations at relatively high resolution. It was constructed by combining the ARPEGE/IFS dynamical core developed at ECMWF and Meteo-France, and the ECHAM5 physical parameterization package that is designed for climate simulations (Yang 2004). The model is characterized by the efficiency advantage of ARPEGE/IFS and may perform extended simulations efficiently even at high resolution. The two models in comparison here thus differ only in physical parameterizations. Two 30-year simulations forced with climatological boundary conditions were carried out using DKCM and ARPEGE at resolution of T63 and 31 vertical layers. The simulations were evaluated using ERA40 re-analysis.

Fig. 1 shows the winter time (DJF) 500 hPa geopotential height (contour lines) and their systematic errors with respect to ERA40 re-analysis (color shadings) for the two models. It can be seen that in extra tropics, the systematic errors in DKCM are generally smaller than that in ARPEGE, in particular in north Pacific-north America sector. The reduction of systematic errors in DKCM compared to ARPEGE is also significant in the zonal mean circulation in upper troposphere and stratosphere (not shown). The wintertime variability (not shown) is also better represented in DKCM than in ARPEGE in comparison with ERA40. The maximum variability in north Atlantic seen in ERA40 is completely missing in ARPEGE, while it is reproduced in DKCM with the maximum area somewhat smaller than seen in ERA40. The above differences may be associated with the differences in diabatic forcing associated with physical parameterizations. Fig. 2 shows the difference of the vertically averaged diabatic forcing between the DKCM and the ARPEGE. Extrema are seen in the northern high latitudes along the edges of sea ice, indicating its cause from the differences in the treatment of sea ice in the two models. In the low and midlatitudes, the major differences between the diabatic forcings in the two models seem to be coincident with the differences between the precipitations in the two models (not shown), implying possible connections with the cloud related process and convective activities. More detailed analyses are undergoing along this line to determine the most crucial physical processes responsible for the above differences in model climatology and variability.

References

Deque, M., 1999: Eulerian versus Semi-Lagrangian in climate simulation: verdict of the nudging technique. CAS/JSC working group on Numerical experimentation: Research Activities in Atmospheric and Oceanic Modelling. Edited by H. Ritchie. Report No. 28. 7.21-7.22.

Ellingson, R. G., J. Ellis and S.B. Feis, 1991: The intercomparison of radiation codes used in

climate models: Longwave results. *J. Geophys. Res.*, 96, 8925-8953.

Held, I. M. and M. J. Suarez, 1994: A proposal for the intercomparison of the dynamical cores of atmospheric general circulation models. *Bull. Amer. Meteor. Soc.*, 75, 1825-1830.

Henderson-Sellers, A., Z.-L. Yang and R.E. Dickinson, 1992: The project for intercomparison of land-surface parameterization schemes. *Bull. Amer. Meteor. Soc.*, 74, 1335-1349.

Shuting Yang, 2004: The DKCM atmospheric model: The atmospheric component of the Danish climate model, Danish Climate Center report 04-05, 23pp.

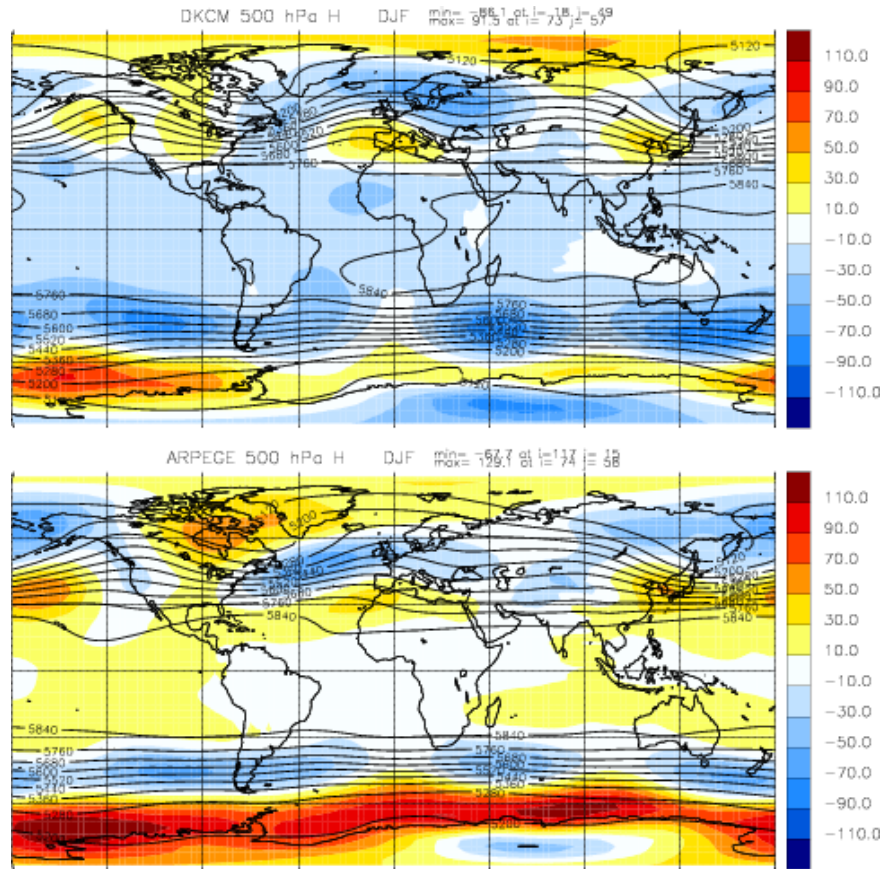


Figure 1. Seasonal mean 500 hPa geopotential height (contour lines) and its systematic errors with respect to ERA40 (color shading) for DJF for DKCM (top) and ARPEGE (middle), respectively. Unit: gpm.

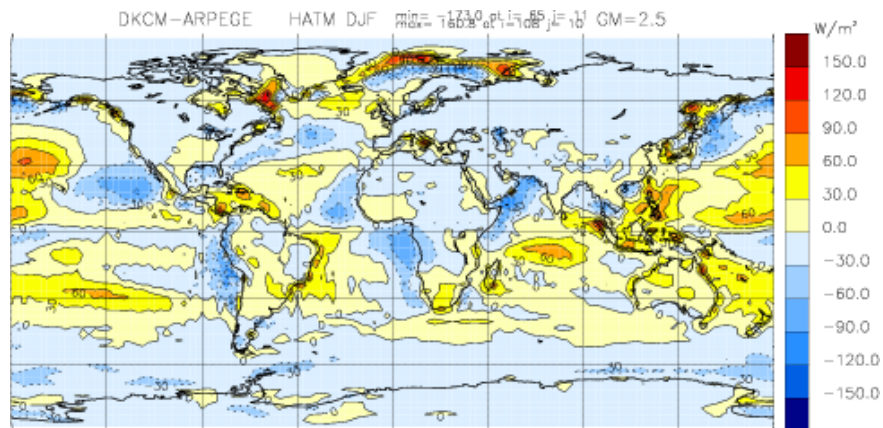


Figure 2. The difference of the vertically averaged diabatic forcing between DKCM and ARPEGE for DJF.
Section 07